Atmos. Chem. Phys. Discuss., doi:10.5194/acp-2016-409, 2016
Manuscript under review for journal Atmos. Chem. Phys.
Published: 26 May 2016

Atmospheric Chemistry and Physics Discussions

Observed microphysical changes in Arctic mixed-phase clouds when transitioning from sea ice to open ocean

G. Young[1], H. M. Jones[1], T. W. Choularton[1], J. Crosier[1,2], K. N. Bower[1], M. W. Gallagher[1], R. S. Davies[3], I. A. Renfrew[3], A. D. Elvidge[4], E. Darbyshire[1], F. Marenco[4], P. R. A. Brown[4], P. J. Connolly[1], G. Lloyd[1,2], P. I. Williams[1,2], J. D. Allan[1,2], J. W. Taylor[1], D. Liu[1], and M. J. Flynn[1]

[1]Centre for Atmospheric Science, University of Manchester, Manchester, UK.
[2]National Centre for Atmospheric Science, University of Manchester, Manchester, UK.
[3]School of Environmental Sciences, University of East Anglia, Norwich, UK.
[4]Met Office, Exeter, UK.

Correspondence to: G. Young (gillian.young@manchester.ac.uk)

Abstract. In situ airborne observations of cloud microphysics, aerosol properties and thermodynamic structure over the transition from sea ice to ocean are presented from the Aerosol-Cloud Coupling and Climate Interactions in the Arctic (ACCACIA) campaign. A case study from 23 March 2013 provides a unique view of the cloud microphysical changes over this transition under cold air outbreak conditions. Cloud base and depth both increased over this transition, and mean droplet number concentrations also increased from approximately 80 cm^{-3} over the sea ice to 90 cm^{-3} over the ocean. The ice properties of the cloud remained approximately constant. Observed ice crystal concentrations averaged approximately 0.5-1.5 L^{-1}, suggesting only primary ice nucleation was active; however, there was evidence of crystal fragmentation at cloud base over the ocean. The liquid-water content increased almost four-fold over the transition and this, in conjunction with the deeper cloud layer, allowed rimed snowflakes to develop which precipitated out of cloud base. Little variation in aerosol particle number concentrations was observed between the different surface conditions; however, some variability with altitude was observed, with notably greater concentrations measured at higher altitudes (>800 m) over the sea ice. Near-surface boundary layer temperatures increased by 13 °C from sea ice to ocean, with corresponding increases in surface heat fluxes and turbulent kinetic energy. These significant thermodynamic changes were concluded to be the primary driver of the microphysical evolution of the cloud. This study represents the first investigation, using in situ airborne observations, of cloud microphysical changes with changing sea ice cover and addresses the question of how the microphysics of Arctic stratiform clouds may change as the region warms and sea ice extent reduces.

1 Introduction

Projected increases in mean temperature due to climate change are greater in the Arctic than the mid-latitudes (ACIA, 2005). Arctic surface temperatures are predicted to rise by up to 7°C by the end of the 21st century (ACIA, 2005). As a consequence of recent warming, observations have shown a prominent decline in sea ice volume over the last thirty years (Serreze et al., 2007), with record-breaking seasonal melts becoming more frequent (e.g. 2004, 2007 and 2012, Stroeve et al., 2005; Perovich

Atmos. Chem. Phys. Discuss., doi:10.5194/acp-2016-409, 2016
Manuscript under review for journal Atmos. Chem. Phys.
Published: 26 May 2016

Atmospheric Chemistry and Physics Discussions

et al., 2008; Parkinson and Comiso, 2013). Observed surface air temperatures have displayed more prominent increases in the winter and spring seasons over the past 100 years (Serreze and Barry, 2011); seasonality which greatly affects the associated sea ice formation and melting processes (e.g. ACIA, 2005; Serreze and Barry, 2011).

It is important to better understand cloud microphysics in the Arctic as clouds contribute significantly towards the Arctic radiative budget (e.g. Intrieri et al., 2002; Shupe and Intrieri, 2004). Arctic clouds often differ from clouds seen at lower latitudes due to differences in aerosol properties and a unique boundary layer structure (Vihma et al., 2014). Additionally, the sea ice is coupled to the Arctic atmosphere and years of decreased summer sea ice extent have coincided with periods of increased cloudiness and humidity during the spring (Kapsch et al., 2013). The relationship between cloud and sea ice fraction adds complexity to the radiative interactions, as increased cloud cover over a low-albedo ocean would typically act to cool the atmosphere through increased reflectivity of incident solar radiation (Curry et al., 1996; Shupe and Intrieri, 2004). However, in the Arctic this incoming shortwave (SW) solar radiation is minimal during the autumn through to spring (Curry et al., 1996), allowing the upward longwave (LW) heat fluxes from the surface to dominate (Intrieri et al., 2002; Palm et al., 2010). The small cloud droplets common in Arctic clouds trap upwelling infra-red radiation efficiently, leading to almost twice the amount of total annual LW radiation than SW radiation at the surface (Curry et al., 1996). Increased springtime cloudiness can therefore lead to increased trapped LW radiation and surface warming, thus potentially affecting the sea ice melting process.

Mixed-phase stratocumulus (MPS) clouds are particularly common in the Arctic (e.g. Pinto, 1998; Shupe et al., 2006; Verlinde et al., 2007). Such clouds are sustained by small vertical motions and are characteristically topped with a liquid layer which facilitates ice formation below (Shupe et al., 2006; Vihma et al., 2014). MPS are particularly prevalent in the transition seasons (Shupe et al., 2006; Morrison et al., 2012). It is uncertain how Arctic cloud fractions will evolve with increased global temperatures (Curry et al., 1996), and comprehending their relationship with sea ice extent is key to improving the representation of radiative interactions in numerical models. Palm et al. (2010) used remote sensing techniques to show that cloudiness typically increases over the marginal ice zone (MIZ) and ocean in comparison to over the sea ice, forming deeper cloud layers with greater optical depth over the ocean. This study also identified increased cloud fractions in years with decreased sea ice cover, implying an important feedback for Arctic warming. Further investigation of cloud properties in the context of surface ice cover could therefore improve both our understanding of the microphysics of high latitude clouds and their dependency on and sensitivity to the surface conditions.

Within global climate models (GCMs), one of the largest sources of uncertainty is our poor understanding of cloud and aerosol processes, particularly so in the polar regions (Boucher et al., 2013). The paucity of observations in the Arctic leads to an inadequate understanding of aerosol-cloud interactions, which in turn impacts our ability to accurately model the cloud microphysics, boundary layer structure and radiative interactions in this region (Curry et al., 1996). There has been a drive to collect more in situ observations of Arctic MPS over recent decades. Studies such as the Mixed-Phase Arctic Cloud Experiment (M-PACE, Verlinde et al., 2007) and the Indirect and Semi-Direct Aerosol Campaign (ISDAC, McFarquhar et al., 2011) collected in situ aircraft observations over the Beaufort Sea near Barrow, Alaska during the transition seasons; autumn 2004 and spring 2008 respectively. These studies have substantially improved our knowledge of transition season Arctic clouds; however, key questions remain. For example, do Arctic clouds differ with geographical location? How do their microphysical

Atmos. Chem. Phys. Discuss., doi:10.5194/acp-2016-409, 2016
Manuscript under review for journal Atmos. Chem. Phys.
Published: 26 May 2016

properties change with a changing surface? Substantial differences in cloud microphysics have been previously identified between three permanent measurement stations in the Canadian Arctic based on meteorological differences (Shupe, 2011) and, given such heterogeneity, studies of other Arctic regions are necessary.

The Aerosol-Cloud Coupling and Climate Interactions in the Arctic (ACCACIA) campaign was carried out to address these questions amongst others. Conducted in the European Arctic in 2013, the ACCACIA project was split into two campaign periods; one in spring (Mar-Apr), the other in summer (Jul-Aug). During the springtime campaign, the Facility for Airborne Atmospheric Measurements (FAAM) BAe-146 atmospheric research aircraft was used to collect high resolution data of cloud and aerosol properties – along with meteorological parameters such as air temperature, humidity and turbulence – in the Svalbard archipelago off the northern coast of Norway. A primary objective of ACCACIA was to investigate both the microphysical properties of MPS in the European Arctic and their relationship with sea ice cover. In this study, detailed observations from one case study are presented to illustrate the changing microphysical structure of clouds with sea ice extent.

2 Instrumentation and data analysis

2.1 FAAM aircraft

The FAAM modified BAe 146-301 Atmospheric Research Aircraft (ARA) is fitted with a suite of aerosol, cloud microphysics and remote sensing instrumentation, detailed by Crosier et al. (2011); Liu et al. (2015) and Lloyd et al. (2015) amongst others. Measurements from these instruments are used here to investigate microphysical properties of clouds in the context of their environment. In this article, all data are expressed as ambient with no standard temperature or pressure corrections applied.

2.1.1 Meteorological instrumentation

The FAAM Core instrument set was active during this campaign (see Renfrew et al., 2008). The GPS-aided Inertial Navigation system and Rosemount temperature sensor are utilised in this study to measure the aircraft's geographical position and the ambient atmospheric temperature respectively. 3D wind components were measured using both a 5-hole turbulence probe and an AIMMS20AQ turbulence probe (Beswick et al., 2008). Dropsondes were released during the campaign to retrieve vertical profiles of the atmospheric temperature and relative humidity (RH), amongst other properties. Additionally, a downward-facing Leosphere ALS450 provided measurements of cloud top height below the aircraft.

2.1.2 Aerosol instrumentation

Sub-micron non-refractory aerosol composition was measured by a Compact Time of Flight Aerosol Mass Spectrometer (C-ToF-AMS, Aerodyne Research Inc., Canagaratna et al., 2007). This instrument has been used extensively in previous aircraft campaigns to characterise such aerosol (e.g. Morgan et al., 2010). Black carbon loadings were monitored with a Single Particle Soot Photometer (SP2, Droplet Measurement Technologies, DMT) and its usage during the ACCACIA campaign is discussed by Liu et al. (2015).

Atmos. Chem. Phys. Discuss., doi:10.5194/acp-2016-409, 2016
Manuscript under review for journal Atmos. Chem. Phys.
Published: 26 May 2016

Fine-mode aerosol particle concentrations (3 nm - 3 µm) were measured using a TSI 3786-LP ultrafine condensation particle counter (CPC). A Passive-Cavity Aerosol Spectrometer Probe (PCASP 100-X, DMT, Rosenberg et al., 2012) was used to count and size accumulation-mode aerosol particles of sizes 0.1 µm to 3 µm. Particle samples (of sizes ∼0.1 µm – 10 µm) were collected on Nuclepore polycarbonate filters exposed from the aircraft for compositional analysis (Young et al., 2016). Additionally, number concentrations and size distributions of aerosol particles and cloud droplets (of sizes 0.6 µm to 50 µm) were measured using the Cloud Aerosol Spectrometer with Depolarisation (CAS-DPOL, DMT, Baumgardner et al., 2001; Glen and Brooks, 2013).

2.1.3 Cloud microphysical instrumentation

Size-resolved cloud droplet concentrations – of sizes 3 µm to 50 µm – were measured with the Cloud Droplet Probe (CDP-100 Version 2, DMT, Lance et al., 2010). These measurements are used to derive the liquid-water content (LWC) of the observed cloud in this study, and this measure is used to distinguish between in- and out-of-cloud observations (using a threshold of $\leq$0.01 g/m^3 for the latter). Additionally, these data are used to compute the mean cloud droplet effective radius within the cloud layers.

The 2-Dimensional Stereo particle imaging probe (2DS, SPEC Inc., Lawson et al., 2006) and Cloud Imaging Probes (CIP15, Baumgardner et al., 2001, and CIP100, DMT) are wing-mounted optical array shadow probes (OAPs) used here to investigate the ice phase of the clouds observed. Processing and analysis of these data has been discussed previously (Crosier et al., 2011, 2014; Taylor et al., 2016). The 2DS images with 10 µm resolution over a size range of 10 µm to 1280 µm, whilst the CIP 15 and CIP 100 provide 15 µm and 100 µm resolution from 15 µm to 930 µm and 100 µm to 6200 µm respectively. The CIP15 also provides additional information with 3-level grey-scale image intensity data, used to improve the correction of over sizing due to depth of field errors. Finally, 8-bit images of cloud particles were taken with 2.3 µm spatial resolution using the Cloud Particle Imager (CPI, SPEC Inc. Lawson et al., 2001). The CPI was not used quantitatively in this study: the small sample volume introduces error into the measurements, manifesting as high local particle concentrations in regions of low ambient number concentrations (Lawson et al., 2001).

2.2 Additional data

Derived cloud top temperature from MODIS satellite retrievals and AVHRR visible satellite imagery are used to illustrate cloud spatial structure and distribution. Additionally, sea ice concentration from NASA's National Snow and Ice Data Centre (NSIDC), derived from passive microwave brightness temperatures (Peng et al., 2013), and the approximate ice concentration from the Met Office Unified Model (MetUM) are used to contextualise the in situ observations.

3 B762: Case study

Flight B762 took place on 23 March 2013. It was a two part flight starting and ending in Kiruna, Sweden, and re-fuelling at Longyearbyen, Svalbard, Norway. Section 1 of the flight was a continuous high-altitude straight, level run (SLR) at approxi-

Atmos. Chem. Phys. Discuss., doi:10.5194/acp-2016-409, 2016
Manuscript under review for journal Atmos. Chem. Phys.
Published: 26 May 2016

Atmospheric Chemistry and Physics Discussions

mately 8000 m, where the lidar was used to sample the cloud structure below. A number of dropsondes were released during this section and the release locations (shown in Fig. 1) allowed for measurements of the atmospheric structure over the varying surface conditions, i.e. open ocean, MIZ and sea ice. The MIZ occurred between approximately 75-76.5°N, north of which a continuous sea ice pack was present. In this study, the MIZ is not distinctly defined; instead, it is approximated by any value between 10% and 90% concentration from NSIDC data as indicated in Fig. 1. Other springtime ACCACIA flights were also designed to investigate changes in atmospheric properties over the transition between sea ice and the ocean; however, flight B762 was the only case which made detailed observations of cloud microphysics over both the sea ice and ocean, and over the transition in between.

Section 2 was split into three parts: a series of SLRs at various altitudes over the sea ice; a sawtooth profile transitioning from sea ice to ocean; and a second set of SLRs over the sea. The flight was designed to investigate the variation in boundary layer structure and cloud over sea ice and the ocean. Low visibility prevented the second set of runs being completed as planned; however, good data coverage of the cloud over the ocean was still achieved.

3.1 Local atmospheric conditions

Cloud layers were observed with the lidar during section 1 of flight B762 (Fig. 2). A continuous layer was observed, where cloud top descended from approximately 1900 m to 1100 m with increasing latitude. Evidence of a lower altitude cloud layer can be seen at high latitudes (500 m at 76.5 °N) through breaks in the continuous layer. The 500 m cloud was not present at lower latitudes (between approximately 73 °N and 73.5 °N), as indicated by the surface echo measured during breaks in the cloud above. An intermittent, high altitude cirrus layer (with optical depth ∼0.5) was seen at various levels from 3000 – 8000 m at higher latitudes on the approach to Longyearbyen.

The structure of the lower troposphere was sampled extensively in section 1 by the 11 dropsondes marked in Fig. 1. A summary of key information from each dropsonde is listed in Table 1. These measurements were collected approximately two hours before and to the west of the in situ cloud observations of section 2; however, the dropsonde and lidar measurements provide a good indication of the structure of the atmosphere during this study.

Figure 3 indicates that the boundary layer structure varied with latitude. At high latitudes over the sea ice (76.5 °N), high relative humidities were recorded in two low-altitude layers at approximately 500 m and 1000 m. At lower latitudes over the ocean (74 °N), a single, deep layer was observed between approximately 300 m and 1200 m. A single temperature inversion was measured by the dropsondes at approximately 1300 m at this latitude. Figures 3**B** and **D** show vertical profiles of Θ and RH data obtained from dropsondes #5 and #11, collected at latitudes comparable to the in situ aircraft runs of section 2. A double potential temperature inversion can be seen over the sea ice (#11), whereas the temperature profile over the ocean indicates that the boundary layer was well-mixed and coupled to the surface (#5). The double temperature inversion over the sea ice is mirrored by twin RH peaks measured at the corresponding altitudes (500 m and 1100 m, #11, Fig. 3**D**), suggesting the presence of two cloud layers $<$1500 m.

Atmos. Chem. Phys. Discuss., doi:10.5194/acp-2016-409, 2016
Manuscript under review for journal Atmos. Chem. Phys.
Published: 26 May 2016

Atmospheric Chemistry and Physics Discussions

Near-surface temperatures sampled by the dropsondes were approximately 13 °C colder to the north over the sea ice (-16.4 °C at ∼77 °N) than over the ocean to the south (-3.4 °C at ∼72 °N, see Table 1). Between the latitudes of the in situ measurements (dropsondes #5 and #11), the difference in near surface temperature is approximately 6 °C.

Figure 4 displays AVHRR visible satellite imagery in panel A and the derived cloud top temperature from MODIS satellite data in panel B. The flight track of section 2 is overlaid to indicate the regions sampled with the aircraft. The high altitude cirrus layer indicated by Fig. 2 can be seen in both of these satellite images. This cirrus cloud was to the north west of the main science region investigated, closer to Spitsbergen. At the locations sampled during the aircraft runs (Fig. 4**B**), there is no clear indication of a higher cirrus cloud layer and the cloud top temperature is approximately -18 °C and -23 °C over the sea ice and ocean regions respectively.

Back trajectory analyses (shown in the Supplement, Fig. S1) indicate that the sampled air came from the north having travelled from northern Canada and/or Greenland, depending on the period of interest. Cold-air outbreak conditions – with off-ice northerly winds of ∼10 ms^{-1} measured within the boundary layer – were maintained for the duration of the science period.

4 In situ observations

4.1 Cloud microphysics

4.1.1 Sea ice

Section 2 of the flight began in Longyearbyen, Svalbard and ended in Kiruna, Sweden. A series of SLRs were performed on an easterly or westerly heading, at an approximately constant latitude. Details of each run are listed in Table 2. Run 7 finished early due to instrument icing as a result of flying in the supercooled mixed phase cloud layer. No additional runs after run 8 were possible as visibility was severely reduced due to below cloud haze. A time series of the microphysical observations is included in the Supplement (Fig. S2).

Figure 5 shows the droplet and ice crystal number concentrations measured over the sea ice by the CDP and 2DS. These measurements indicate the presence of a mixed-phase cloud between approximately 300 m and 700 m, with mean droplet and ice number concentrations of approximately 90 cm^{-3} and 1 L^{-1} respectively at ∼400 m. 2DS ice concentrations agree well with the CIP15 (shown in Fig. S2). Derived mean CDP LWC peaks at ∼0.05 g/m^3 at 400 m, where the mean temperature is -19°C. The double temperature inversion suggested by the sea ice dropsondes in Fig. 3 can also be seen here at 600 m and 1100 m, though not as clearly. The secondary cloud layer at ∼1000 m, indicated by the dual RH peaks in Figs. 3**C** and **D**, is subtly detected; however, it is not as significant as the main layer observed and had likely dissipated somewhat from the time of the dropsonde measurements.

During these sea ice SLRs, the aim was to measure below, in and above the cloud layer. The lowest altitude case (run 2) was carried out in a fog layer present between cloud base and the surface. This fog was only present over the sea ice region. As described by Young et al. (2016), aircraft filters were exposed during this run, and a silicate dust concentration of ∼0.3 cm^{-3}

Atmos. Chem. Phys. Discuss., doi:10.5194/acp-2016-409, 2016
Manuscript under review for journal Atmos. Chem. Phys.
Published: 26 May 2016

Atmospheric Chemistry and Physics Discussions

was measured. This concentration, in conjunction with the cloud top temperature (-19.7°C), was used to evaluate the Niemand et al. (2012, hereafter N12) primary ice nucleation parameterisation. Predicted ice number concentrations were approximately 0.7 L^{-1} (yellow square, Fig. 5**B**). Dust concentrations of double and triple that measured were also used to evaluate N12 to test sensitivity to this input (orange and brown square respectively, Fig. 5**B**). The shape of the dust surface area distribution was maintained and the number concentration in each bin was scaled accordingly. The DeMott et al. (2010, hereafter D10) primary ice parameterisation was also evaluated using these filter measurements, giving an ice nucleating particle (INP) concentration of 0.9 L^{-1}. In Fig. 5**B**, evaluations of D10 using filter (yellow), PCASP (pink) and CAS-DPOL (grey) data are shown. Inputs and outputs of these parameterisations are detailed in Table 3.

Longitudinally-separated data from runs 2, 3 and 4 are displayed in Fig. S3. The cloud was observed to be spatially inhomogeneous. Cloud particle concentrations increase at similar geographical locations indicating that the same cloud layer was sampled at the different altitudes. Run 5 was conducted above the cloud layer to characterise aerosol size distributions and composition. However, ice crystals were observed, and images collected by the CPI towards the end of this run are shown in Fig. 6. Pristine bullet-rosettes were observed, indicating that these crystals had fallen from a greater height without interaction with liquid cloud.

Figures 5**C(a-d)** show the number size distributions measured along each SLR carried out over the sea ice. A droplet mode at ∼10 µm can be seen in Figs. 5**C(a-c)** – corresponding to the in-cloud runs (runs 2-4) – with the CAS-DPOL and CDP measurements. This mode is distinctly missing from the run 5 data; negligible droplet concentrations were observed at this altitude, with ice crystals dominating overall particle concentrations.

4.1.2 Ocean

Figure 7 shows the droplet and ice crystal number concentrations for the ocean section of the flight. Over the ocean, the cloud layer extends from 700 m to 1500 m. CDP LWC displays a more consistent profile in this section, with a mean value of ∼0.3 g/m^3 measured between approximately 1100 m and 1400 m. 2DS ice crystal data do not follow the same trend as the droplet data, with variable concentrations measured at each altitude bin.

Run 7 was conducted within the cloud layer and probe icing was noted. The ice number concentrations from this run are not substantially greater than any of the others, suggesting this icing problem may not have greatly affected the measurements; however, there is an increased CIP100 mode within the number size distributions (at sizes >100 µm, Fig. 7**B**) which is not mirrored by the CIP15.

This cloud is more homogeneous in the liquid phase than the layer measured over the sea ice (Fig. S4), with consistent droplet concentrations and LWC values (∼70 cm^{-3} and 0.3 g/m^3 respectively) measured with changing longitude during each run. As with the sea ice SLRs, a clear droplet mode is visible at approximately 10 µm in runs 6 and 7 (Figs. 7**C(a,b)**). This mode is not clear in run 8; this run was carried out at low altitude below cloud to collect aerosol data. However, as with run 5, some ice was measured by the 2DS, CIP100 and CIP15 (Figs. 7, S2, S4). Images from the CIP100 during run 8 are shown in Fig. 8; large dendritic crystals are present, with notable riming, of sizes ∼1-1.6 mm. Their size and structure suggests interaction with cloud droplets within cloud, subsequent growth and eventual precipitation as snow.

Atmos. Chem. Phys. Discuss., doi:10.5194/acp-2016-409, 2016
Manuscript under review for journal Atmos. Chem. Phys.
Published: 26 May 2016

Atmospheric Chemistry and Physics Discussions

High ice number concentrations were measured between 700 m and 900 m at cloud base. Size distributions from the microphysics probes during this period are shown in Fig. 7**C(d)**: an enhanced secondary mode of ice crystals $\geq$100 µm is observed, along with a broadened CDP distribution. The mean temperature measured was approximately -16 °C and numerous large dendrites were observed; large, fragile crystals which may fragment easily upon collision. CIP100 images of these crystals are shown in Fig. S5. 2DS ice crystal concentrations increase to a mean value of approximately 5 L^{-1}; much greater than the mean concentration observed within the mixed cloud layer ($\sim$1 L^{-1}).

The D10 parameterisation was again evaluated using below-cloud aerosol measurements in conjunction with the cloud top temperature (-20.1 °C). Evaluated ice predictions using PCASP (pink) and CAS-DPOL (grey) data from run 8 are shown in panel B at 250 m, overlaying the blocked out altitudes. Predicted INP concentrations were 2.23 L^{-1} and 1.28 L^{-1} respectively (see Table 3). No filter data are available over the ocean.

4.1.3 Transition region

Several profiles were flown in a sawtooth over the transition region from the sea ice to open ocean. Profile 5 was conducted over sea ice; profiles 6 and 7 were over the MIZ; and profile 8 was over the ocean (see Table 4).

Figure 9 shows the CDP droplet number concentrations and derived LWC from each profile, with altitude and mean droplet effective radius overlaid in the top and bottom rows respectively. These data show a clear lifting and deepening of the cloud layer when transiting from sea ice to open ocean. Mean in-cloud droplet number concentrations increase from about 100 cm^{-3} to 150 cm^{-3} through the transition, whilst the corresponding mean LWC and droplet effective radii increase from 0.1 g/m^3 to 0.4 g/m^3 and 5 µm to 8-10 µm respectively.

Figure 10 shows the 2DS and CIP100 ice concentrations measured over the transition region. Evaluations of the D10 parameterisation – using PCASP and CAS-DPOL data and the coldest temperature measured in each profile – are also shown. Ice number concentrations measured by each instrument remain consistent over the transition, with a mean number concentration of approximately 0.1 L^{-1} measured by the CIP100 over the sea ice and ocean. A slight decrease in the mean 2DS ice concentration can be seen from sea ice to ocean, from approximately 1.5 L^{-1} to 0.5 L^{-1}. The lifting and deepening of the liquid cloud layer seen in Fig. 9 is not apparent with these ice data. The CIP100 in particular shows a contrasting trend; increasing concentrations below cloud toward the surface suggests precipitation as snow from the cloud layers above. The measured concentrations marginally increase over the ocean, and this precipitation is observed over a greater altitude range due to the lifting of cloud base.

The double temperature inversion indicated in the dropsonde data (Fig. 3) can be viewed in the first two profiles. The lower inversion is eroded to produce a clear, single inversion at $\sim$1400 m during the last profile over the ocean. The gradient of the temperature profile decreases over the ocean due to surface warming, whilst the cloud top temperature remains approximately -20 °C with the changing surface.

Atmos. Chem. Phys. Discuss., doi:10.5194/acp-2016-409, 2016
Manuscript under review for journal Atmos. Chem. Phys.
Published: 26 May 2016

Atmospheric Chemistry and Physics Discussions

4.2 Aerosol

Aerosol number concentrations measured by the various probes on board the aircraft are reported in Table 5. CPC particle concentrations are greater at high altitudes (>800 m) over both surfaces, as is the total concentration recorded by the PCASP over sea ice. The gradient in CPC concentration is greatest over the ocean, with a high altitude measurement of over 4 × that measured at low altitude. These number concentrations are not observed to the same extent in the PCASP data.

Over the ocean, the concentrations measured by the PCASP (both total and >0.5 µm) and CAS-DPOL are approximately constant with altitude. Concentrations of large aerosol (which may act as ice nucleating particles, d>0.5 µm) are approximately uniform with altitude over the ocean. Over the sea ice, a greater loading of coarse-mode aerosol is measured nearer the surface and this consistency with altitude is not observed.

In general, the number concentrations measured over the ocean are lower than over the sea ice. Figure 11 displays the size distributions from the PCASP and CAS-DPOL split into high and low altitude data. Small particles measured by the PCASP (0.1 µm<d<0.5 µm) reach a greater concentration over the sea ice than over the ocean. Low altitude CAS-DPOL concentrations over the sea ice are heightened with comparison to the high altitude data; it is possible that swollen aerosol particles associated with the fog layer were being measured, enhancing the number concentration. Such particles may not be removed from the data using the CDP LWC $\leq$0.01 g/m^3 out-of-cloud threshold applied here. Over ocean, data from both instruments are more comparable; however, the low altitude PCASP data show a greater loading across most sizes.

Non-refractory sub-micron aerosol composition measured by the AMS is shown in Fig. 12. Technical issues prevented continuous measurement over the ocean, with problems occurring during run 7 especially. The measured nitrate mass loading remains low and consistent throughout. The sulphate loading is variable with altitude, especially over the transition region between ice and ocean. Higher mass loadings are measured at higher altitudes ($\sim$1 µg/m^3 at 1400 m): increasing during the last SLR over the sea ice (run 5), the signal becomes highly variable over the sawtooth profile. Such variability is also observed in the organic and ammonium traces. PCASP particle number and SP2 black carbon (BC) mass observations follow the same trends throughout the science period, both mirror the same sinusoidal pattern over the MIZ. Both signals are variable, with increases observed at high altitudes, but no distinct differences are observed between sea ice and ocean measurements.

4.3 Boundary layer dynamics

Turbulent kinetic energy (TKE) and sensible and latent heat fluxes measured along the flight path are shown in Fig. 13. Approximate MetUM ice concentration is shown in the left-hand and middle columns. Over the sea ice, both the sensible and latent heat fluxes and the TKE remain relatively constant at about 0 W m^{-2} and 0.5 m^2 s^{-2} respectively. More variability is observed in these three parameters over the ocean. Sensible heat fluxes range from -20 to 0 W m^{-2} at low altitude over the sea ice, whilst substantially greater values of >30 W m^{-2} are observed over the ocean, with >100 W m^{-2} measured in some instances. A similar difference is observed with the latent heat fluxes with variable measurements of approximately 50 W m^{-2} over the ocean, contrasting observations of $\sim$0 W m^{-2} over the sea ice. Low altitude ($\sim$350 m) TKE increases from approximately 0-0.5 m^2 s^{-2} to 1.5 m^2 s^{-2} over the transition. TKE, sensible heat fluxes and latent heat fluxes all increase and

Atmos. Chem. Phys. Discuss., doi:10.5194/acp-2016-409, 2016
Manuscript under review for journal Atmos. Chem. Phys.
Published: 26 May 2016

Atmospheric Chemistry and Physics Discussions

become more variable over the MIZ and ocean with comparison to the sea ice, with the greatest values typically observed at low altitude over the ocean.

The turbulence and AIMMS probes recorded vertical velocity throughout the science period. The turbulence probe suffered some icing effects during runs 7 and 8, whilst the AIMMS probe collected no data for run 8 due to a technical issue. Averaged PDFs from over the sea ice and ocean are shown in Fig. 14. The turbulence probe and AIMMS PDFs compare well. The sea ice PDF displays little variation, with the majority of measurements lying close to the mean value. Maxima and minima of the distribution are approximately $\pm 1\,\mathrm{ms}^{-1}$. In comparison, the ocean PDFs are significantly broader, with more variability from the mean observed. Maxima and minima of the ocean PDF extend to $\pm 2\,\mathrm{ms}^{-1}$ and the distribution is skewed toward updraughts.

5 Discussion

5.1 Sea ice

The averaged data over sea ice point toward a low-altitude cloud with a low liquid water content (Fig. 5). Ice crystal concentrations are spatially variable within the cloud (Fig. S3) yet they are consistent, suggesting only primary ice nucleation was active. The temperature within the cloud was between -18°C and -20°C (Fig. 5); far below the range required for secondary ice production (e.g. Hallett and Mossop, 1974).

Data from runs 2, 3 and 4 depict a typical Arctic cloud structure (e.g. Verlinde et al., 2007; Morrison et al., 2012; Vihma et al., 2014): a liquid-layer at cloud top, with ice formation and aggregation below. Such processes are inferred from the relative quantities of ice crystals measured by the 2DS and CIP100 instruments (Fig. S3), as the latter can measure much larger ice crystals than the former.

Run 5 was planned to be an above cloud aerosol run; however, the 2DS and CIP100 instruments detect notable ice concentrations to the western end of the run (Fig. S3). This suggests that precipitation was being sampled from a higher cloud layer, possibly the high altitude cirrus layer observed closer to Spitsbergen (Figs. 2 and 4). Additionally, RH data from the high-latitude dropsondes (Fig. 3**C**) indicate the possibility of a higher cloud layer ($\sim$2000 m – 3000 m) in this region. CPI ice crystal images during run 5 (Fig. 6) also point towards the sampling of another cloud, as the imaged bullet rosettes typically form at higher, colder altitudes and aggregate as they descend. This ice precipitation was observed to the west of and was separate to the main cloud layer sampled over the sea ice, and thus was excluded from the comparison with the ocean cloud layer.

Observed aerosol concentrations varied substantially with altitude over the sea ice. Results show elevated sulphate, PCASP, CPC and BC measurements during run 5 (Table 5 and Fig. 12); the latter of which is consistent with the Asian BC plumes identified during the ACCACIA campaign (Liu et al., 2015). These plumes contained an average BC mass loading of $\sim$27 ng s m^{-3} during flight B762, consistent with the low altitude measurements here (Fig. 12). Similarly, this mass loading is also equivalent to the annual median BC concentration measured at Zeppelin, Svalbard over the period 1998-2007 (Eleftheriadis et al., 2009).

Atmos. Chem. Phys. Discuss., doi:10.5194/acp-2016-409, 2016
Manuscript under review for journal Atmos. Chem. Phys.
Published: 26 May 2016

Atmospheric Chemistry and Physics Discussions

PCASP data do not increase as much as the CPC data at high altitudes, suggesting either a pollution layer characterised by small particle sizes (3 nm<d<0.1 µm) or new particle formation at these heights.

More large particles are measured close to the sea ice surface, as shown by the >0.5 µm PCASP and CAS-DPOL measurements (Table 5). This suggests contributions of primary particle emissions from the surface. A large fraction of these low altitude particles were sea salt (Young et al., 2016), which could have been transported from the nearby ocean or lofted into the atmosphere by near-surface winds over polynyas or leads in the sea ice. Additionally, frost flowers could be a possible surface source of modified sea-salt aerosol (Xu et al., 2013); however, their characteristic signature would not be detectable by the analysis presented by Young et al. (2016).

Observed ice crystal concentrations vary little over the sea ice, with slight increases toward cloud base attributable to aggregation and precipitation out of the cloud. Using the D10 parameterisation, predicted INP concentrations were 0.9 L^{-1}, 1.90 L^{-1} and 3.31 L^{-1} for aerosol concentrations measured by the aircraft filters (Young et al., 2016), PCASP, and CAS-DPOL respectively (listed in Table 3). The filter data produce best agreement with the mean 2DS ice concentration in the mixed cloud layer. D10 predictions using the probe data overestimate with comparison to the mean ice concentrations observed in the cloud; an overestimation which can be explained by incorrectly assuming that all predicted INPs nucleate to form ice crystals. The large fraction of coarse-mode sea salt particles identified over the sea ice (Young et al., 2016) would be unlikely to contribute to the INP population as these are inefficient INPs. Despite this, given the uncertainties in the parameterisation itself, these predictions do well to replicate the ice observed in the cloud.

For comparison, N12 was evaluated with the dust size distribution derived from the aircraft filters (Table 3). As discussed by Young et al. (2016), this dust loading is likely under-represented as a result of the analysis technique and collection efficiency issues. Evaluations of N12 with measured, double and triple dust loadings all compare well – within the 1 σ range shown (Fig. 5) – with the run 2 ice data, illustrating a lack of sensitivity to this input. Both the N12 and D10 parameterisations perform best when implementing the filter data: these data predict a lower ice number than observed, yet these inputs are likely an under-representation of the true atmospheric dust and accumulation-mode aerosol concentrations due to the technique used (Young et al., 2016). Therefore, it can be speculated that the ice number concentrations observed over the sea ice may be explained by the dust loadings collected.

Over the sea ice, the liquid-water content is low (~0.03 g/m^3, Fig. 5**A**) and the mean droplet radius is small (~4-5 µm, Fig. 9), with droplet number concentrations of approximately 70-90 cm^{-3}. It is possible that the cloud layer interacted with aerosol from above, via entrainment processes, as suggested by the presence of numerous small cloud droplets; with more CCN available, more cloud droplets can form (Jackson et al., 2012). Mean droplet number concentrations from the CDP (Fig. 5) are consistent with both the high and low altitude PCASP number concentrations measured (Table 5), further suggesting that the ambient aerosol mixed with the cloud layer from above and below.

The vertical velocity PDFs (Fig. 14) and TKE (Fig. 13) suggest that the boundary layer over the sea ice is stable with relatively little mixing compared to downstream. Little variability and low values are observed in the measured TKE, sensible heat flux, and latent heat flux (Fig. 13). The potential temperature profiles from the dropsondes (Fig. 3) also indicate weakly stable stratification with very strong temperature inversions, emphasising that boundary layer mixing was inhibited over the

Atmos. Chem. Phys. Discuss., doi:10.5194/acp-2016-409, 2016
Manuscript under review for journal Atmos. Chem. Phys.
Published: 26 May 2016

Atmospheric Chemistry and Physics Discussions

sea ice. A lack of substantial vertical air motions may explain the low LWC; by the Bergeron-Findeisen mechanism, the ice crystals act as a sink for vapour in the cold temperatures observed (∼-20 °C). This causes the suppression of the liquid phase – via a suppressed supersaturation – and cloud droplets remain small and fewer in number.

5.2 Marginal ice zone

When transitioning from sea ice to ocean, both cloud depth and cloud base increase (Fig. 9). The most significant change in cloud microphysics over the transition is in the liquid phase, where both the droplet number and mean size – and consequently, the liquid-water content – increase dramatically (Fig. 9). The mean CDP LWC increases by almost 4× at cloud top, from approximately 0.1 g/m^3 to 0.4 g/m^3. Increased cloud depth, droplet concentration and mean droplet effective radius imply an increased optical thickness and albedo of the cloud over the ocean (Twomey, 1974), thus it would reflect more incident SW radiation than the sea ice cloud. However, as upward LW radiation dominates in the Arctic spring, these ocean clouds would contribute towards a net warming at the surface; a net warming that could enhance the melting of the nearby sea ice (Palm et al., 2010). Radiative interactions between the sea ice cloud and the surface are more difficult to interpret due to a lack of both substantial surface heat fluxes and incoming SW radiation.

The ambient temperatures experienced within the cloud layers (Fig. 10) remain colder than required for secondary ice production and warmer than the homogeneous freezing threshold throughout. The observed 2DS ice crystal concentrations are consistently low – approximately 0.5-1.5 L^{-1} – throughout the transition, again indicating that only primary ice nucleation was active. Higher ice concentrations are observed at high altitudes (up to 2 L^{-1} at ∼1350 m) over the sea ice, suggesting that some precipitation was again measured from a higher cloud layer. This agrees with the conclusion from run 5, as both this profile and run 5 were conducted close together (1400 m) and to the west (∼26.5-27 °E) of the main science region. Though some seeding from above is probable in both run and profile 5, the ice concentrations measured during the SLRs over sea ice and ocean – and the remaining profiles over the MIZ – suggest that this is not the case for the majority of these data.

Predicted ice number concentrations using the D10 parameterisation are shown in Fig. 10 at the altitude of the temperature inversion in each profile. At the beginning and end of the sawtooth profile, the prediction using PCASP data gives good agreement with the observations. Over the sea ice, CAS-DPOL data must be interpreted with caution due to the fog layer sampled. In the middle of the sawtooth profile, predicted concentrations using PCASP and CAS-DPOL data do not agree as well with the observations. However, the predicted values are still within the uncertainty associated with the parameterisation.

The sulphate, organic, ammonium and BC loadings vary almost sinusoidally with altitude over the transition region, with maxima reached at the peaks of the sawtooth profile (Fig. 12). These peaks occur above the cloud layer, as indicated in Fig. 9. These species commonly act as CCN in the atmosphere and could be acting to increase the cloud droplet number concentration across the MIZ. There is no evidence that the organic species influences the ice phase, as the former varies significantly whereas the latter remains approximately constant. The observed increases in mass loading are small, as are the increases in number concentration measured by the PCASP (Fig. 12), therefore it is unlikely that they are the cause of the significant microphysical changes observed.

Atmos. Chem. Phys. Discuss., doi:10.5194/acp-2016-409, 2016
Manuscript under review for journal Atmos. Chem. Phys.
Published: 26 May 2016

Measured surface heat fluxes – both sensible and latent – become more variable and increase over the transition to ocean, with greatest values measured at low altitudes (<1000 m). The approximate MetUM ice fraction indicated in Fig. 13 mirrors the transition of this variability, with little deviation from 0 W m^{-2} measured when sea ice is present and significant variability developing over the open water. Similar changes are observed in the TKE data, where increased turbulence is induced as the air mass moves over the comparatively warm ocean.

5.3 Ocean

Between sea ice and ocean, the most prominent microphysical difference observed is in the liquid phase; the liquid-water content of this cloud is significantly greater than over the sea ice. The observed cloud is deeper, with a mean LWC of ∼0.4 g/m^3 and droplet number concentration of ∼80-100 cm^{-3} (Fig. 7). Observed ice crystal number concentrations within the oceanic cloud are similar to those measured over the sea ice (0.5-1 L^{-1}) and the D10 INP predictions are in reasonable agreement (∼1-2 L^{-1}, Fig. 7). These measurements are consistent with altitude; however, there is an increase at the base of the mixed cloud layer (∼700 – 900 m). This increase could be due to sedimentation of ice crystals or low sampling statistics at these altitudes. However, the presence of dendritic ice crystals (Fig. S5) combined with an ice concentration of ∼5 L^{-1}, a mean temperature of approximately -16 °C, and an enhanced ice crystal mode in the size distributed data (Fig. 7**C(d)**) suggests that ice-ice collisions may have taken place at cloud base (Rangno and Hobbs, 2001). The ambient temperatures were too low to suggest secondary ice formation via the Hallet-Mossop pathway (Hallett and Mossop, 1974), but it is likely that some crystal fragmentation due to collisions enhanced the observed primary ice concentration at this altitude.

Probe icing was an issue during run 7 and this effect can be seen in the sharp increase in CIP100 and corresponding decrease in the 2DS ice concentrations in Fig. 7**C(b)**. Run 8 was intended to be a low altitude, below cloud run; however, precipitation particles were again observed. Contrasting run 5, this precipitation is related to the observed ocean cloud layer sampled above during runs 6 and 7. Images from the CIP100 (Fig. 8) indicate that these particles are large and rimed, inferring an interaction with liquid droplets within the mixed layer above.

Aerosol data were not available for a significant fraction of the ocean component of the flight. Despite this, it can still be seen that the mass loadings of all AMS-measured species are low in this region (Fig. 12). The measured BC loading is more variable over the ocean than the sea ice or MIZ, varying from approximately 10 ng/m^3 to 100 ng/m^3. This variability is mirrored by the particle number concentration measured by the PCASP. The heightened BC loadings are consistent with the monthly average reported by Eleftheriadis et al. (2009) for Feb/Mar at Zeppelin station, Svalbard (∼80 ng/m^3).

There is also consistency between the high and low altitude measurements from the CAS-DPOL and PCASP (>0.5 µm) over the ocean, suggesting a constant vertical profile of large aerosol in this region. Aerosol number concentrations were found to be lower in general over the ocean than over the sea ice. Therefore, there is a lack of evidence for a significant surface flux of aerosol particles over the ocean that may have affected the cloud microphysics. No aircraft filters were exposed over the ocean; therefore, the composition of this coarse-mode aerosol could not be established.

From Fig. 3, the atmosphere is notably warmer over the ocean than over the sea ice. There is a steady increase in the boundary layer potential temperature measured by the dropsondes from north to south. The changes in the Θ profiles are

Atmos. Chem. Phys. Discuss., doi:10.5194/acp-2016-409, 2016
Manuscript under review for journal Atmos. Chem. Phys.
Published: 26 May 2016

most prominent in the boundary layer, with less variability observed >1500 m. The near-surface temperature inferred by the dropsondes increases by 13 °C between the most northerly and southerly latitudes sampled. Over the transition from sea ice to ocean, the inferred temperature difference at the surface was ∼6 °C. The ocean surface was therefore significantly warmer than the sea ice, and this sharp temperature gradient affected the both structure of the boundary layer and any clouds that formed within it.

The broader vertical wind PDFs over the ocean (Fig. 14) suggest increased turbulence levels and mixing within the boundary layer. This is in agreement with Figs. 3 and 13: the surface temperature increased with transition from the frozen sea ice to the warm ocean, thus increasing sensible heat and latent heat fluxes from the surface. At low altitude over the ocean, both of these measures routinely exceeded 20 W m^{-2}, whilst they remained consistent at approximately 0 W m^{-2} over the sea ice. Measured TKE was significantly higher at low altitude over the ocean than over the sea ice, suggesting a much more turbulent boundary layer over the open water. The contrast between the observed cloud microphysics over sea ice and ocean is most likely due to these increased fluxes and induced turbulent motions. The warmer, more turbulent boundary layer promotes the formation of more cloud droplets and allows them to grow to larger sizes (Fig. 9) via sustained supersaturations, thus feeding the liquid phase such that it can better compete with the ice phase in the cloud.

5.4 Study comparison

The microphysics of the cloud observed over the sea ice has more in common with the cirrus case observed during the M-PACE campaign (Verlinde et al., 2007) – with a similar LWC and mean droplet radius measured – than the M-PACE stratocumulus case. In addition, the cirrus case reported by Verlinde et al. (2007) was observed at a similar temperature (approximately -20°C) as the sea ice cloud observed here. The close proximity to the cold sea ice surface could be causing this cloud to behave like a cirrus, decoupled cloud: with little-to-no surface sensible and latent heat fluxes affecting the cloud (with little variability from 0 W m^{-2} observed), the resultant microphysics may evolve as it would higher up in the troposphere. In contrast, the microphysics of the cloud observed over the ocean is more comparable with recent Arctic studies of single-layer stratocumulus (e.g. McFarquhar et al., 2007; Verlinde et al., 2007; Jackson et al., 2012). The cloud over the ocean was deeper and of a greater optical depth than the sea ice case, agreeing with the observations of Palm et al. (2010).

Mean droplet number concentrations varied from approximately 80 cm^{-3} over the sea ice to approximately 90 cm^{-3} over the ocean. These concentrations were variable with altitude within each cloud layer. These values are consistent with the first ACCACIA spring case reported by Lloyd et al. (2015) but not the second: as also concluded by the authors, their second spring case was subjected to a higher aerosol loading which enhanced the droplet number concentration of the cloud. Consistency between the liquid phase in this study; spring case 1 from Lloyd et al. (2015); and the MPS observations reported by other Arctic studies (e.g. Verlinde et al., 2007; Jackson et al., 2012) suggests that droplet number concentrations of ∼150 cm^{-3} or below are common amongst Arctic mixed-phase single-layer stratocumulus in the transition seasons. Mean droplet effective radii over the sea ice are comparable to previous springtime Arctic studies (e.g. 5.7 µm, Earle et al., 2011), whilst the larger effective radii measured over the ocean agree better with observations of autumnal Arctic single- and multi-layer clouds (e.g. approximately 10 µm and 8–13 µm respectively, Klein et al., 2009; Morrison et al., 2009). These latter observations were conducted over

Atmos. Chem. Phys. Discuss., doi:10.5194/acp-2016-409, 2016
Manuscript under review for journal Atmos. Chem. Phys.
Published: 26 May 2016

the ocean close to Barrow, Alaska; therefore, these large droplet sizes may be a common occurrence in ocean-based clouds observed in cold-air outbreak scenarios such as these.

The ice phase is approximately constant across the transition from sea ice to ocean. Again, these measurements agree well with the springtime ACCACIA cases presented by Lloyd et al. (2015): the ice concentrations are variable and can reach up to $\sim$10 L^{-1} (identified here to be due to crystal fragmentation), yet they are low on average (0.5-1.5 L^{-1}) throughout the mixed cloud layer. The sea ice cloud observed here would fall into the Type IV category established by Rangno and Hobbs (2001), as it was characterised by droplet concentrations of $\sim$100 cm^{-3}, small droplet effective radii, and only a few ice crystals per litre of air. The ocean cloud borders on the Type V category, with larger droplet sizes and precipitation developing; however, the droplet and ice number concentrations are still in better agreement with the Type IV criteria. One could postulate that the continued development of the ocean cloud over the warm ocean, with further growth of even larger cloud droplets that might subsequently freeze, could allow the cloud layer to evolve into a Type V cloud, with more ice and less liquid. The microphysical characteristics of these clouds may be more susceptible to cloud glaciation and break up via the Bergeron-Findeisen mechanism. Such clouds have been previously observed in the Arctic during the M-PACE campaign in the autumn of 2004 (e.g. Rangno and Hobbs, 2001; McFarquhar et al., 2007), with higher ice crystal (mean of 2.8$\pm$6.9 L^{-1} for mixed-phase single-layer stratus, McFarquhar et al., 2007) and lower droplet number concentrations than reported here. From these differences, one might infer that the M-PACE clouds were simply further developed than those observed in this study, or that there may be some influence from either different geographical aerosol sources or seasonal dependencies. Results from the ISDAC campaign may address the geographical hypothesis, as ice crystal and cloud droplet concentrations of approximately 0.5-1.5 L^{-1} and $\sim$150 cm^{-3} were observed over broken sea ice during the early spring at Barrow, Alaska (Apr 2008 McFarquhar et al., 2011; Jackson et al., 2012). These concentrations are comparable to those detailed here; however, the ISDAC clouds were much warmer, with cloud top temperatures ranging from -15 °C to -12 °C. The microphysical consistency between these clouds observed in different locations may suggest that a similar source of INPs is influencing these clouds, or that the ice phase is not highly sensitive to variability in aerosol properties between different locations. Variability in droplet number between different measurement locations can be more easily explained via pollution events for example, such as that observed by Lloyd et al. (2015).

The Arctic Study of Tropospheric Aerosol and Radiation (ASTAR) campaign also made cloud observations in the vicinity of Svalbard; however, much higher ice crystal concentrations (up to 50 L^{-1}) were observed (May 2004, Gayet et al., 2009). This phenomenon was explained by Hallet-Mossop secondary ice production. Ice enhancement due to crystal collisions was inferred at cloud base over the ocean here, but the temperature was consistently too cold to allow for secondary ice via the Hallet-Mossop pathway. The lack of dominating secondary ice in the Arctic clouds studied here is again consistent with McFarquhar et al. (2011), Jackson et al. (2012) and Lloyd et al. (2015), leading to the conclusion that the MPS present in the Arctic during early spring are typically too cold for this phenomenon, irrespective of their geographical location. Primary ice nucleation was found to be solely responsible for the ice in the clouds examined here, whilst secondary ice formation has been found to play a greater role in the late spring and summer (Gayet et al., 2009; Lloyd et al., 2015).

Atmos. Chem. Phys. Discuss., doi:10.5194/acp-2016-409, 2016
Manuscript under review for journal Atmos. Chem. Phys.
Published: 26 May 2016

Atmospheric Chemistry and Physics Discussions

6 Conclusions

In situ aircraft observations of cloud microphysics, aerosol properties and boundary layer structure have been presented from the Aerosol-Cloud Coupling and Climate Interactions in the Arctic (ACCACIA) campaign. Using data from one case study (flight B762, 23 March 2013, Fig. 1), we have shown how the microphysics of mixed-phase stratiform clouds can significantly change over the transition from sea ice to ocean. This study represents the first investigation of in situ, measured cloud microphysical changes over this transition, and offers insight into how the microphysics of Arctic stratiform clouds may change with decreasing sea ice extent in the future.

The conclusions of this study are as follows:

- Cloud microphysics changed significantly from sea ice to ocean; cloud base lifted and cloud depth increased over the transition (Figs. 5, 7, 9). Both cloud droplet number and mean size increased and, consequently, the LWC increased by almost 4× from sea ice to ocean. Mean cloud droplet effective radii increased from approximately 5 µm to 8-10 µm over the transition, producing a cloud over the ocean with greater optical and geometrical thickness, and increased albedo. The ocean cloud would likely reflect incoming SW radiation more efficiently than the sea ice cloud; however, as SW radiation is low during the Arctic spring, it is more likely that this cloud layer would instead contribute towards warming at the surface by trapping upwelling LW radiation.

- The boundary layer warmed significantly from sea ice to ocean, with a near-surface temperature difference of 13 °C observed between the most northerly and southerly latitudes sampled (Fig. 3). Increased surface fluxes, vertical motion and turbulent activity (Figs. 13 and 14) infer substantially more mixing in the boundary layer over the ocean than over the sea ice. This is concluded to be the cause of the microphysical changes observed during this case study, as the increased heat and turbulence likely promoted the formation and growth of more cloud droplets within the cloud layer.

- The predominant change in cloud microphysics was in the liquid-phase, suggesting a similar source of INPs in both regimes. Observed ice concentrations were low and remained low over the transition (Fig. 10), suggesting only primary ice formation was active. However, evidence of crystal fragmentation was observed at cloud base over the ocean (Fig. 7), leading to minor contributions of secondary ice. The ice crystals were typically found to be larger over the ocean than over the sea ice. Such crystals were observed below cloud over the ocean as rimed snowflakes, precipitating out of the cloud (Fig. 8). Predicted ice crystal concentrations using the DeMott et al. (2010) and Niemand et al. (2012) parameterisations compared well with the ice observations over the sea ice and ocean (Figs. 5 and 7), and agreed to within the uncertainty attributed to the parameterisations themselves (approximately an order of magnitude).

- Good agreement was identified between the ice crystal number concentrations measured in this study and those reported from the ISDAC campaign; both campaigns observed mean ice concentrations of approximately 0.5-1.5 L^{-1} during the early spring at different locations within the Arctic Circle. This consistency suggests that geographically-dependent aerosol sources may not have a prominent influence on the ice phase of the clouds. In contrast, substantial microphysical

Atmos. Chem. Phys. Discuss., doi:10.5194/acp-2016-409, 2016
Manuscript under review for journal Atmos. Chem. Phys.
Published: 26 May 2016

differences were identified between this study and previous late spring (ASTAR), summer (ACCACIA) and autumnal (M-PACE) studies, emphasising that seasonality remains a crucial factor in the study of Arctic cloud microphysics.

These in situ observations offer a good test case for cloud-resolving and weather prediction model validations in the Arctic. Investigating the influence of the surface on cloud microphysics in such models, and studying how sensitive the simulated clouds are to changes in both surface and aerosol properties, could allow us to improve our understanding of how the cloud microphysics of Arctic stratiform clouds may adapt and respond to our warming climate.

Acknowledgements. This work was funded by the National Environment Research Council [NERC], under grant NE/I028696/1, as part of the ACCACIA campaign. G. Young was supported by a NERC PhD studentship. We would like to thank everyone involved in the ACCACIA project. Airborne data were obtained using the BAe-146-301 Atmospheric Research Aircraft [ARA] flown by Directflight Ltd and managed by the Facility for Airborne Atmospheric Measurements [FAAM], which is a joint entity of the Natural Environment Research Council [NERC] and the Met Office. MODIS data were accessed via the NASA LAADS Web Archive. Sea ice data were obtained from the National Snow and Ice Data Centre [NSIDC].

Atmos. Chem. Phys. Discuss., doi:10.5194/acp-2016-409, 2016
Manuscript under review for journal Atmos. Chem. Phys.
Published: 26 May 2016

Atmospheric Chemistry and Physics Discussions

References

ACIA: Arctic Climate Impact Assessment, pp. 990–1020, Cambridge University Press, 2005.

Baumgardner, D., Jonsson, H., Dawson, W., O'Connor, D., and Newton, R.: The cloud, aerosol and precipitation spectrometer: a new instrument for cloud investigations, Atmospheric Research, 59–60, 251 – 264, doi:10.1016/S0169-8095(01)00119-3, 13th International Conference on Clouds and Precipitation, 2001.

Beswick, K. M., Gallagher, M. W., Webb, A. R., Norton, E. G., and Perry, F.: Application of the Aventech AIMMS20AQ airborne probe for turbulence measurements during the Convective Storm Initiation Project, Atmospheric Chemistry and Physics, 8, 5449–5463, doi:10.5194/acp-8-5449-2008, 2008.

Boucher, O., Randall, D., Artaxo, P., Bretherton, C., Feingold, G., Forster, P., Kerminen, V. M., Kondo, Y., Liao, H., Lohmann, U., Rasch, P., Satheesh, S. K., Sherwood, S., Stevens, B., and Zhang, X. Y.: Clouds and Aerosols, in: Climate Change 2013: The Physical Science Basis. Contribution of Working Group I to the Fifth Assessment Report of the Intergovernmental Panel on Climate Change, edited by: Stocker, T. F., Qin, D., Plattner, G. K., Tignor, M., Allen, S. K., Boschung, J., Nauels, A., Xia, Y., Bex, V., and Midgley, P. M., Cambridge University Press, Cambridge, United Kingdom and New York, NY, USA, doi:10.1017/CBO9781107415324.016, 2013.

Canagaratna, M., Jayne, J., Jimenez, J., Allan, J., Alfarra, M., Zhang, Q., Onasch, T., Drewnick, F., Coe, H., Middlebrook, A., Delia, A., Williams, L., Trimborn, A., Northway, M., DeCarlo, P., Kolb, C., Davidovits, P., and Worsnop, D.: Chemical and microphysical characterization of ambient aerosols with the aerodyne aerosol mass spectrometer, Mass Spectrometry Reviews, 26, 185–222, doi:10.1002/mas.20115, 2007.

Crosier, J., Bower, K. N., Choularton, T. W., Westbrook, C. D., Connolly, P. J., Cui, Z. Q., Crawford, I. P., Capes, G. L., Coe, H., Dorsey, J. R., Williams, P. I., Illingworth, A. J., Gallagher, M. W., and Blyth, A. M.: Observations of ice multiplication in a weakly convective cell embedded in supercooled mid-level stratus, Atmospheric Chemistry & Physics, 11, 257–273, doi:10.5194/acp-11-257-2011, 2011.

Crosier, J., Choularton, T. W., Westbrook, C. D., Blyth, A. M., Bower, K. N., Connolly, P. J., Dearden, C., Gallagher, M. W., Cui, Z., and Nicol, J. C.: Microphysical properties of cold frontal rainbands, Quarterly Journal of the Royal Meteorological Society, 140, 1257–1268, doi:10.1002/qj.2206, 2014.

Curry, J. A., Rossow, W. B., Randall, D., and Schramm, J. L.: Overview of Arctic Cloud and Radiation Characteristics., Journal of Climate, 9, 1731–1764, doi:10.1175/1520-0442(1996)009<1731:OOACAR>2.0.CO;2, 1996.

DeMott, P. J., Prenni, A. J., Liu, X., Kreidenweis, S. M., Petters, M. D., Twohy, C. H., Richardson, M. S., Eidhammer, T., and Rogers, D. C.: Predicting global atmospheric ice nuclei distributions and their impacts on climate, Proceedings of the National Academy of Sciences, doi:10.1073/pnas.0910818107, 2010.

Earle, M. E., Liu, P. S. K., Strapp, J. W., Zelenyuk, A., Imre, D., McFarquhar, G. M., Shantz, N. C., and Leaitch, W. R.: Factors influencing the microphysics and radiative properties of liquid-dominated Arctic clouds: Insight from observations of aerosol and clouds during ISDAC, Journal of Geophysical Research (Atmospheres), 116, D00T09, doi:10.1029/2011JD015887, 2011.

Eleftheriadis, K., Vratolis, S., and Nyeki, S.: Aerosol black carbon in the European Arctic: Measurements at Zeppelin station, Ny-Ålesund, Svalbard from 1998-2007, Geophysics Research Letters, 36, L02809, doi:10.1029/2008GL035741, 2009.

Gayet, J.-F., Treffeisen, R., Helbig, A., Bareiss, J., Matsuki, A., Herber, A., and Schwarzenboeck, A.: On the onset of the ice phase in boundary layer Arctic clouds, Journal of Geophysical Research (Atmospheres), 114, D19201, doi:10.1029/2008JD011348, 2009.

Glen, A. and Brooks, S. D.: A new method for measuring optical scattering properties of atmospherically relevant dusts using the Cloud and Aerosol Spectrometer with Polarization (CASPOL), Atmospheric Chemistry & Physics, 13, 1345–1356, doi:10.5194/acp-13-1345-2013, 2013.

Hallett, J. and Mossop, S. C.: Production of Secondary Ice Particles during the Riming Process, Nature, 249, 26–28, doi:10.1038/249026a0, 1974.

Intrieri, J. M., Fairall, C. W., Shupe, M. D., Persson, P. O. G., Andreas, E. L., Guest, P. S., and Moritz, R. E.: An annual cycle of Arctic surface cloud forcing at SHEBA, Journal of Geophysical Research (Oceans), 107, 8039, doi:10.1029/2000JC000439, 2002.

Jackson, R. C., McFarquhar, G. M., Korolev, A. V., Earle, M. E., Liu, P. S. K., Lawson, R. P., Brooks, S., Wolde, M., Laskin, A., and Freer, M.: The dependence of ice microphysics on aerosol concentration in arctic mixed-phase stratus clouds during ISDAC and M-PACE, Journal of Geophysical Research (Atmospheres), 117, D15207, doi:10.1029/2012JD017668, 2012.

Kapsch, M.-L., Graversen, R. G., and Tjernström, M.: Springtime atmospheric energy transport and the control of Arctic summer sea-ice extent, Nature Clim. Change, 3, 744–748, doi:10.1038/nclimate1884, 2013.

Klein, S. A., McCoy, R. B., Morrison, H., Ackerman, A. S., Avramov, A., Boer, G. d., Chen, M., Cole, J. N. S., Del Genio, A. D., Falk, M., Foster, M. J., Fridlind, A., Golaz, J.-C., Hashino, T., Harrington, J. Y., Hoose, C., Khairoutdinov, M. F., Larson, V. E., Liu, X., Luo, Y., McFarquhar, G. M., Menon, S., Neggers, R. A. J., Park, S., Poellot, M. R., Schmidt, J. M., Sednev, I., Shipway, B. J., Shupe, M. D., Spangenberg, D. A., Sud, Y. C., Turner, D. D., Veron, D. E., Salzen, K. v., Walker, G. K., Wang, Z., Wolf, A. B., Xie, S., Xu, K.-M., Yang, F., and Zhang, G.: Intercomparison of model simulations of mixed-phase clouds observed during the ARM Mixed-Phase Arctic Cloud Experiment. I: Single-layer cloud, Quarterly Journal of the Royal Meteorological Society, 135, 979–1002, doi:10.1002/qj.416, 2009.

Lance, S., Brock, C. A., Rogers, D., and Gordon, J. A.: Water droplet calibration of the Cloud Droplet Probe (CDP) and in-flight performance in liquid, ice and mixed-phase clouds during ARCPAC, Atmospheric Measurement Techniques, 3, 1683–1706, doi:10.5194/amt-3-1683-2010, 2010.

Lawson, R. P., Baker, B. A., Schmitt, C. G., and Jensen, T. L.: An overview of microphysical properties of Arctic clouds observed in May and July 1998 during FIRE ACE, Journal of Geophysical Research, 106, 14 989, doi:10.1029/2000JD900789, 2001.

Lawson, R. P., O'Connor, D., Zmarzly, P., Weaver, K., Baker, B., Mo, Q., and Jonsson, H.: The 2D-S (Stereo) Probe: Design and Preliminary Tests of a New Airborne, High-Speed, High-Resolution Particle Imaging Probe, Journal of Atmospheric and Oceanic Technology, 23, 1462, doi:10.1175/JTECH1927.1, 2006.

Liu, D., Quennehen, Darbyshire, E., Allan, J. D., Williams, P. I., Taylor, J. W., Bauguitte, S. J., B., Flynn, M. J., Gallagher, M. W., Bower, K. N., Choularton, T. W., and Coe, H.: The importance of Asia as a source of black carbon to the European Arctic during springtime 2013, Atmospheric Chemistry & Physics, 15, 14 843–14 887, doi:doi:10.5194/acp-15-11537-2015, 2015.

Lloyd, G., Choularton, T. W., Bower, K. N., Crosier, J., Jones, H., Dorsey, J. R., Gallagher, M. W., Connolly, P., Kirchgaessner, A. C. R., and Lachlan-Cope, T.: Observations and comparisons of cloud microphysical properties in spring and summertime Arctic stratocumulus during the ACCACIA campaign, Atmospheric Chemistry & Physics, 15, 3719–3737, doi:10.5194/acp-15-3719-2015, 2015.

McFarquhar, G. M., Zhang, G., Poellot, M. R., Kok, G. L., McCoy, R., Tooman, T., Fridlind, A., and Heymsfield, A. J.: Ice properties of single-layer stratocumulus during the Mixed-Phase Arctic Cloud Experiment: 1. Observations, Journal of Geophysical Research (Atmospheres), 112, D24201, doi:10.1029/2007JD008633, 2007.

McFarquhar, G. M., Ghan, S., Verlinde, J., Korolev, A., Strapp, J. W., Schmid, B., Tomlinson, J. M., Wolde, M., Brooks, S. D., Cziczo, D., Dubey, M. K., Fan, J., Flynn, C., Gultepe, I., Hubbe, J., Gilles, M. K., Laskin, A., Lawson, P., Leaitch, W. R., Liu, P., Liu, X., Lubin, D., Mazzoleni, C., MacDonald, A.-M., Moffet, R. C., Morrison, H., Ovchinnikov, M., Shupe, M. D., Turner, D. D., Xie, S., Zelenyuk,

A., Bae, K., Freer, M., and Glen, A.: Indirect and Semi-direct Aerosol Campaign: The Impact of Arctic Aerosols on Clouds., Bull. Am. Meteorol. Soc., 92, 183–201, doi:10.1175/2010BAMS2935.1, 2011.

Morgan, W. T., Allan, J. D., Bower, K. N., Highwood, E. J., Liu, D., McMeeking, G. R., Northway, M. J., Williams, P. I., Krejci, R., and Coe, H.: Airborne measurements of the spatial distribution of aerosol chemical composition across Europe and evolution of the organic fraction, Atmospheric Chemistry and Physics, 10, 4065–4083, doi:10.5194/acp-10-4065-2010, 2010.

Morrison, H., McCoy, R. B., Klein, S. A., Xie, S., Luo, Y., Avramov, A., Chen, M., Cole, J. N. S., Falk, M., Foster, M. J., Del Genio, A. D., Harrington, J. Y., Hoose, C., Khairoutdinov, M. F., Larson, V. E., Liu, X., McFarquhar, G. M., Poellot, M. R., von Salzen, K., Shipway, B. J., Shupe, M. D., Sud, Y. C., Turner, D. D., Veron, D. E., Walker, G. K., Wang, Z., Wolf, A. B., Xu, K.-M., Yang, F., and Zhang, G.: Intercomparison of model simulations of mixed-phase clouds observed during the ARM Mixed-Phase Arctic Cloud Experiment. II: Multilayer cloud, Quarterly Journal of the Royal Meteorological Society, 135, 1003–1019, doi:10.1002/qj.415, 2009.

Morrison, H., de Boer, G., Feingold, G., Harrington, J., Shupe, M. D., and Sulia, K.: Resilience of persistent Arctic mixed-phase clouds, Nature Geoscience, 5, 11–17, doi:10.1038/ngeo1332, 2012.

Niemand, M., Möhler, O., Vogel, B., Vogel, H., Hoose, C., Connolly, P., Klein, H., Bingemer, H., DeMott, P., Skrotzki, J., and Leisner, T.: A Particle-Surface-Area-Based Parameterization of Immersion Freezing on Desert Dust Particles, Journal of Atmospheric Sciences, 69, 3077–3092, doi:10.1175/JAS-D-11-0249.1, 2012.

Palm, S. P., Strey, S. T., Spinhirne, J., and Markus, T.: Influence of Arctic sea ice extent on polar cloud fraction and vertical structure and implications for regional climate, Journal of Geophysical Research (Atmospheres), 115, D21209, doi:10.1029/2010JD013900, 2010.

Parkinson, C. L. and Comiso, J. C.: On the 2012 record low Arctic sea ice cover: Combined impact of preconditioning and an August storm, Geophys. Res. Lett., 40, 1356–1361, doi:10.1002/grl.50349, 2013.

Peng, G., Meier, W. N., Scott, D. J., and Savoie, M. H.: A long-term and reproducible passive microwave sea ice concentration data record for climate studies and monitoring, Earth System Science Data, 5, 311–318, doi:10.5194/essd-5-311-2013, 2013.

Perovich, D. K., Richter-Menge, J. A., Jones, K. F., and Light, B.: Sunlight, water, and ice: Extreme Arctic sea ice melt during the summer of 2007, Geophysics Research Letters, 35, L11501, doi:10.1029/2008GL034007, 2008.

Pinto, J. O.: Autumnal Mixed-Phase Cloudy Boundary Layers in the Arctic., Journal of Atmospheric Sciences, 55, 2016–2038, doi:10.1175/1520-0469(1998)055<2016:AMPCBL>2.0.CO;2, 1998.

Rangno, A. L. and Hobbs, P. V.: Ice particles in stratiform clouds in the Arctic and possible mechanisms for the production of high ice concentrations, Journal of Geophysical Research: Atmospheres, 106, 15 065–15 075, doi:10.1029/2000JD900286, 2001.

Renfrew, I. A., Moore, G. W. K., Kristjánsson, J. E., Ólafsson, H., Gray, S. L., Petersen, G. N., Bovis, K., Brown, P. R. A., Føre, I., Haine, T., Hay, C., Irvine, E. A., Lawrence, A., Ohigashi, T., Outten, S., Pickart, R. S., Shapiro, M., Sproson, D., Swinbank, R., Woolley, A., and Zhang, S.: The Greenland Flow Distortion experiment, Bull. Amer. Meteorol. Soc., 89, 1307–1324, doi:10.1175/2008BAMS2508.1, 2008.

Rosenberg, P. D., Dean, A. R., Williams, P. I., Dorsey, J. R., Minikin, A., Pickering, M. A., and Petzold, A.: Particle sizing calibration with refractive index correction for light scattering optical particle counters and impacts upon PCASP and CDP data collected during the Fennec campaign, Atmospheric Measurement Techniques, 5, 1147–1163, doi:10.5194/amt-5-1147-2012, 2012.

Serreze, M. C. and Barry, R. G.: Processes and impacts of Arctic amplification: A research synthesis, Global and Planetary Change, 77, 85 – 96, doi:10.1016/j.gloplacha.2011.03.004, 2011.

Serreze, M. C., Holland, M. M., and Stroeve, J.: Perspectives on the Arctic's Shrinking Sea-Ice Cover, Science, 315, 1533–, doi:10.1126/science.1139426, 2007.

Shupe, M. D.: Clouds at Arctic Atmospheric Observatories. Part II: Thermodynamic Phase Characteristics, Journal of Applied Meteorology and Climatology, 50, 645–661, doi:10.1175/2010JAMC2468.1, 2011.

Shupe, M. D. and Intrieri, J. M.: Cloud Radiative Forcing of the Arctic Surface: The Influence of Cloud Properties, Surface Albedo, and Solar Zenith Angle., Journal of Climate, 17, 616–628, doi:10.1175/1520-0442(2004)017<0616:CRFOTA>2.0.CO;2, 2004.

Shupe, M. D., Matrosov, S. Y., and Uttal, T.: Arctic Mixed-Phase Cloud Properties Derived from Surface-Based Sensors at SHEBA., Journal of Atmospheric Sciences, 63, 697–711, doi:10.1175/JAS3659.1, 2006.

Stroeve, J. C., Serreze, M. C., Fetterer, F., Arbetter, T., Meier, W., Maslanik, J., and Knowles, K.: Tracking the Arctic's shrinking ice cover: Another extreme September minimum in 2004, Geophys. Res. Lett., 32, L04 501, doi:10.1029/2004GL021810, 2005.

Taylor, J. W., Choularton, T. W., Blyth, A. M., Liu, Z., Bower, K. N., Crosier, J., Gallagher, M. W., Williams, P. I., Dorsey, J. R., Flynn, M. J., Bennett, L. J., Huang, Y., French, J., Korolev, A., and Brown, P. R. A.: Observations of cloud microphysics and ice formation during COPE, Atmospheric Chemistry and Physics, 16, 799–826, doi:10.5194/acp-16-799-2016, 2016.

Twomey, S.: Pollution and the planetary albedo, Atmospheric Environment, 8, 1251 – 1256, doi:10.1016/0004-6981(74)90004-3, 1974.

Verlinde, J., Harrington, J. Y., McFarquhar, G. M., Yannuzzi, V. T., Avramov, A., Greenberg, S., Johnson, N., Zhang, G., Poellot, M. R., Mather, J. H., Turner, D. D., Eloranta, E. W., Zak, B. D., Prenni, A. J., Daniel, J. S., Kok, G. L., Tobin, D. C., Holz, R., Sassen, K., Spangenberg, D., Minnis, P., Tooman, T. P., Ivey, M. D., Richardson, S. J., Bahrmann, C. P., Shupe, M., Demott, P. J., Heymsfield, A. J., and Schofield, R.: The Mixed-Phase Arctic Cloud Experiment, Bulletin of the American Meteorological Society, 88, 205, doi:10.1175/BAMS-88-2-205, 2007.

Vihma, T., Pirazzini, R., Fer, I., Renfrew, I. A., Sedlar, J., Tjernström, M., Lüpkes, C., Nygård, T., Notz, D., Weiss, J., Marsan, D., Cheng, B., Birnbaum, G., Gerland, S., Chechin, D., and Gascard, J. C.: Advances in understanding and parameterization of small-scale physical processes in the marine Arctic climate system: a review, Atmospheric Chemistry & Physics, 14, 9403–9450, doi:10.5194/acp-14-9403-2014, 2014.

Xu, L., Russell, L. M., Somerville, R. C. J., and Quinn, P. K.: Frost flower aerosol effects on Arctic wintertime longwave cloud radiative forcing, J. Geophys. Res., 118, 13 282–13 291, doi:10.1002/2013JD020554, 2013.

Young, G., Jones, H. M., Darbyshire, E., Baustian, K. J., McQuaid, J. B., Bower, K. N., Connolly, P. J., Gallagher, M. W., and Choularton, T. W.: Size-segregated compositional analysis of aerosol particles collected in the European Arctic during the ACCACIA campaign, Atmospheric Chemistry and Physics, 16, 4063–4079, doi:10.5194/acp-16-4063-2016, 2016.

Atmos. Chem. Phys. Discuss., doi:10.5194/acp-2016-409, 2016
Manuscript under review for journal Atmos. Chem. Phys.
Published: 26 May 2016

Atmospheric Chemistry and Physics Discussions

Table 1. Key dropsonde information.

Sonde	Latitude [°N]	Longitude [°E]	Temperature[a] [°C]	Surface Condition[b]
1	72.2	21.6	-3.4	Ocean
2	72.9	22.2	-4.4	Ocean
3	73.9	23.3	-7.3	Ocean
4	74.4	23.9	-9.3	Ocean
5	75.0	24.5	-10.5	Ocean
6	75.4	25.2	-12.3	Ocean
7	75.7	25.5	-13.3	MIZ
8	75.9	25.9	-14.2	MIZ
9	76.2	26.2	-14.7	Sea ice
10	76.4	26.6	-15.0	Sea ice
11	76.8	27.3	-16.4	Sea ice

MIZ: Marginal Ice Zone.
[a]Near-surface ambient atmospheric temperature.
[b]Based on NSIDC daily average sea ice concentration.

Table 2. Straight and level run information. Values quoted are arithmetic mean quantities, with 1σ quoted in brackets.

Run	Start time [UTC]	End time [UTC]	Direction	Altitude[a] [m]	Temperature[b] [°C]	% in cloud[c]	Latitude [°N]	Surface Condition
2	12:45:39	13:00:00	W to E	377 (6)	-18.5 (0.2)	11.7	76.8	Sea ice
3	13:03:07	13:12:06	E to W	477 (5)	-19.2 (0.4)	27.0	76.8	Sea ice
4	13:16:03	13:26:10	W to E	612 (3)	-19.7 (0.2)	17.8	76.8	Sea ice
5	13:30:15	13:41:33	E to W	1435 (4)	-19.9 (0.3)	0	76.8	Sea ice
6	14:15:20	14:25:16	W to E	1449 (6)	-19.4 (0.9)	14.7	74.8	Ocean
7	14:28:19	14:35:09	E to W	1190 (56)	-19.6 (0.3)	92.0	74.8	Ocean
8	14:42:39	14:52:46	W to E	378 (5)	-12.3 (0.1)	0	74.8	Ocean

[a]Derived from GPS measurements.
[b]Ambient temperature measured with the Rosemount de-iced temperature sensor.
[c]In cloud defined as when CDP LWC $\geq$0.01 g/m^3.

Atmos. Chem. Phys. Discuss., doi:10.5194/acp-2016-409, 2016
Manuscript under review for journal Atmos. Chem. Phys.
Published: 26 May 2016

Atmospheric Chemistry and Physics Discussions

Table 3. Summary of inputs to and evaluations of the D10 (DeMott et al., 2010) and N12 (Niemand et al., 2012) parameterisations. Silicate dust concentrations – derived from filter analysis presented by Young et al. (2016) – are used to evaluate N12. No filter data are available over the ocean.

Surface Condition	Parameterisation	Temperature [°C]	Aerosol Input	$N_{aerosol}$ [cm^{-3}]	N_{ice} [L^{-1}]
Sea ice	N12	-19.7	Filter[a]	0.3	0.7[b]
	N12	-19.7	2×Filter[a]	0.7	1.3[b]
	N12	-19.7	3×Filter[a]	1.0	2.0[b]
	D10	-19.7	Filter[c]	0.6	0.9
	D10	-19.7	PCASP[c]	2.00	1.90
	D10	-19.7	CAS-DPOL[c]	6.85	3.31
Ocean	D10	-20.1	PCASP[c]	2.72	2.23
	D10	-20.1	CAS-DPOL[c]	1.11	1.28

[a] Silicate dust concentration.
[b] Derived frozen fraction applied to dust distribution.
[c] Aerosol concentration >0.5 µm.

Table 4. Sawtooth profile information.

Profile	Time [UTC]		Altitude [m]		Latitude [°N]		Temperature [°C]	
	Start	End	Start	End	Start	End	Min	Max
5	13:43:37	13:52:15	1423	47	76.6	76.1	-21.2	-15.0
6	13:52:15	13:57:50	43	1450	76.1	75.8	-20.7	-14.9
7	13:57:50	14:09:27	1459	42	75.8	75.1	-21.7	-9.4
8	14:09:28	14:14:32	43	1469	75.1	74.8	-21.3	-9.3

Atmos. Chem. Phys. Discuss., doi:10.5194/acp-2016-409, 2016
Manuscript under review for journal Atmos. Chem. Phys.
Published: 26 May 2016

Atmospheric Chemistry and Physics Discussions

Table 5. Background aerosol information, split into high (>800 m) and low altitude (<800 m) data over the respective surfaces. Arithmetic mean values of number concentration (cm^{-3}) are reported, with one standard deviation in brackets.

Instrument	High altitude over ice	Low altitude over ice	High altitude over sea	Low altitude over sea
CPC	351.0 (410.2)	133.4 (34.0)	595.0 (836.8)	129.0 (68.2)
PCASP	109.4 (57.2)	86.2 (21.1)	41.2 (31.4)	48.3 (22.0)
PCASP (>0.5 µm)	0.95 (4.76)	1.94 (4.97)	0.17 (1.62)	0.54 (3.85)
CAS-DPOL	1.27 (3.72)	11.2 (19.7)	2.48 (7.82)	2.27 (7.29)

Atmos. Chem. Phys. Discuss., doi:10.5194/acp-2016-409, 2016
Manuscript under review for journal Atmos. Chem. Phys.
Published: 26 May 2016

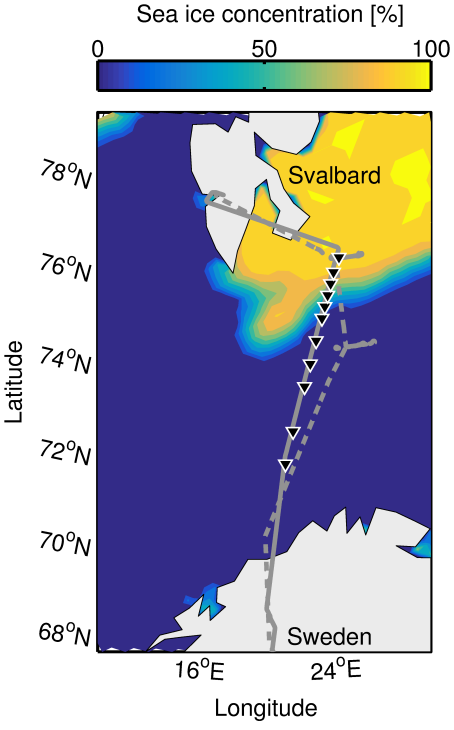

Figure 1. Flight track for B762 on 23 March 2013 over sea ice concentration (shading). Section 1 of the flight (grey, solid) was conducted at a high altitude, where 11 dropsondes (black triangles) were released. Section 2 of the flight (grey, dashed) conducted straight, level runs over the sea ice and open water, with a sawtooth profile over the transition region.

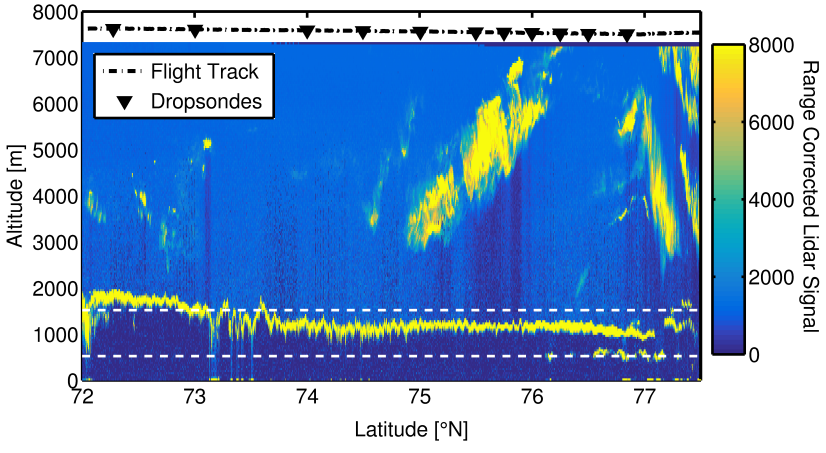

Figure 2. Lidar signal from section 1 of the flight. Aircraft altitude is indicated (black) and each dropsonde release point is marked (downward-facing triangles). White dotted lines are shown at 500 m and 1500 m for ease of comparison with the in situ observations.

Atmos. Chem. Phys. Discuss., doi:10.5194/acp-2016-409, 2016
Manuscript under review for journal Atmos. Chem. Phys.
Published: 26 May 2016

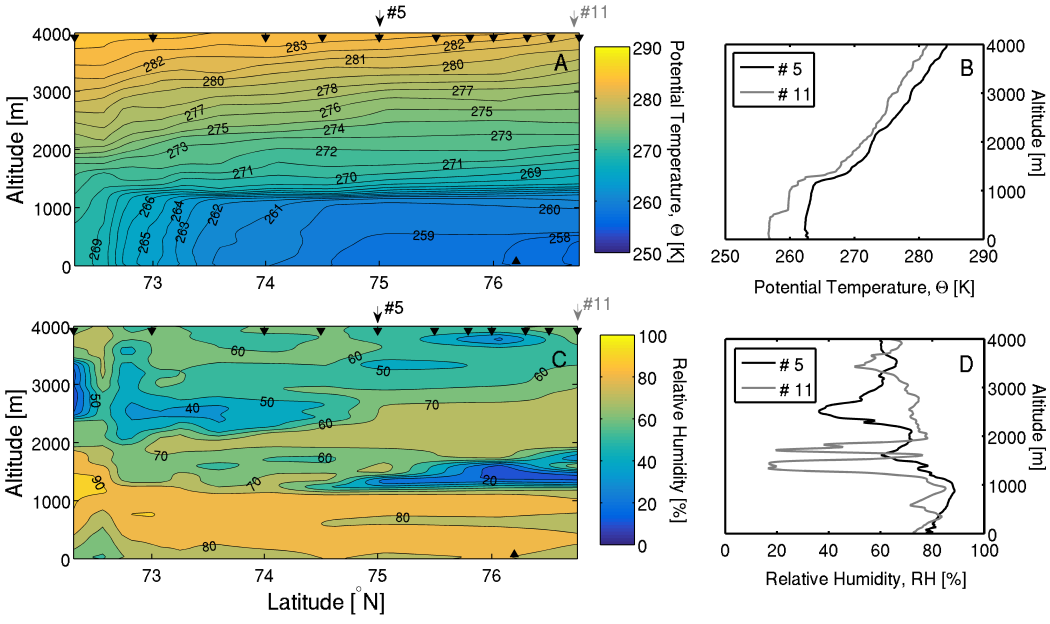

Figure 3. Contour figures of potential temperature (Θ, **panel A**) and relative humidity (RH, **panel C**) using data from the 11 dropsondes released on approach to Longyearbyen, Svalbard. Dropsonde release locations (downward-facing triangles) and the approximate sea ice edge (upward-facing triangle) are marked. Profiles of Θ (**panel B**) and RH (**panel D**) from dropsondes #5 and #11 are also shown due to their comparable latitudes to the in situ observations (see Table 1). The positions of these dropsondes relative to the others are indicated above **panels A** and **C**.

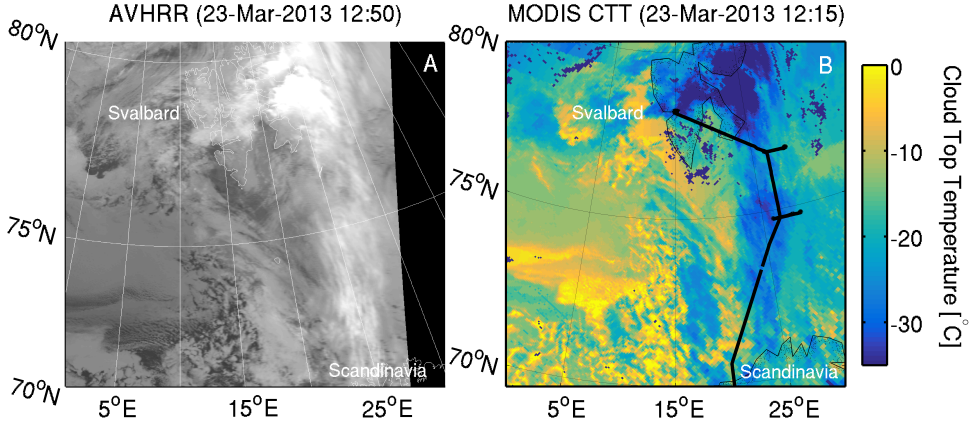

Figure 4. AVHRR visible satellite image (**panel A**) and cloud top temperature (CTT) derived from MODIS retrievals (**panel B**) at times close to the start of section 2 of B762. Section 2 of the flight track is indicated (black) in panel B.

Atmos. Chem. Phys. Discuss., doi:10.5194/acp-2016-409, 2016
Manuscript under review for journal Atmos. Chem. Phys.
Published: 26 May 2016

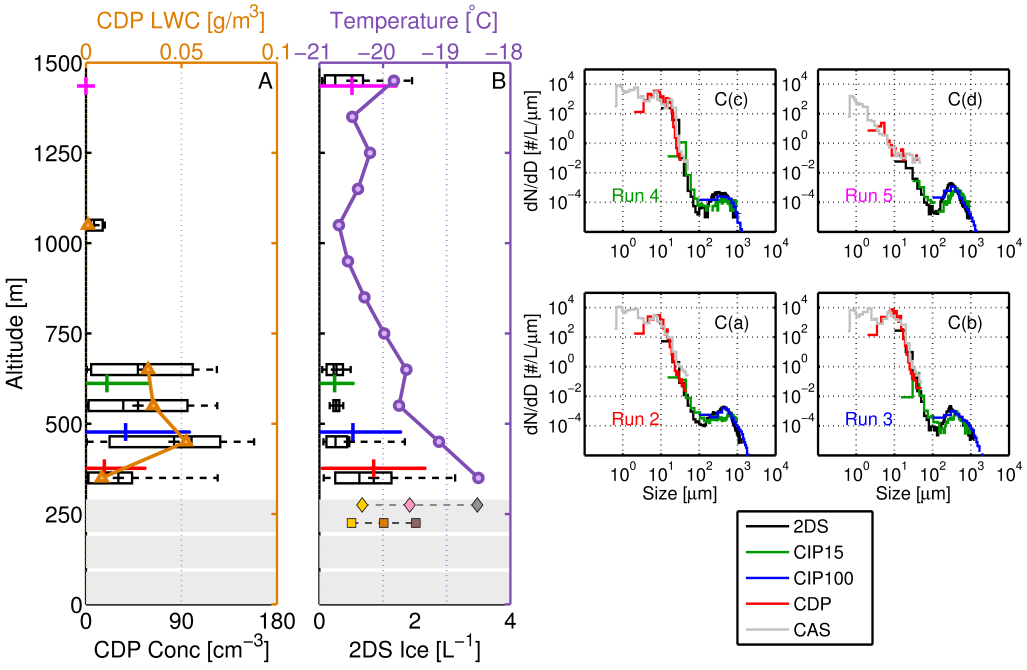

Figure 5. Microphysics summary of averaged observations over the sea ice. **A:** CDP droplet number concentration (boxes, black) with derived liquid-water content overlaid (orange). **B:** 2DS ice crystal number concentration (boxes, black) with mean temperature measured overlaid (purple). Only CDP and 2DS data $>0.5\,\mathrm{cm}^{-3}$ and $>0.05\,\mathrm{L}^{-1}$ respectively have been included. Box edges represent the 25$^{\mathrm{th}}$ and 75$^{\mathrm{th}}$ percentiles, and the median and mean values are denoted by | and + respectively. Altitudes not sampled are blocked out ($\leq$300m). **A** and **B**: number concentrations from each SLR are shown in colour at each corresponding altitude (run 2: red, run 3: blue, run 4: green, run 5: magenta). Arithmetic means are indicated (|) with each horizontal bar extending to $\pm 1\sigma$. **B:** Evaluated D10 and N12 parameterisations are shown (diamonds and squares, respectively) overlaying the blocked out altitudes (see text). **C(a-d):** Number size distributions (dN/dD) from each SLR over the sea ice (runs 2-5 respectively). Legend refers to panel **C** only.

Atmos. Chem. Phys. Discuss., doi:10.5194/acp-2016-409, 2016
Manuscript under review for journal Atmos. Chem. Phys.
Published: 26 May 2016

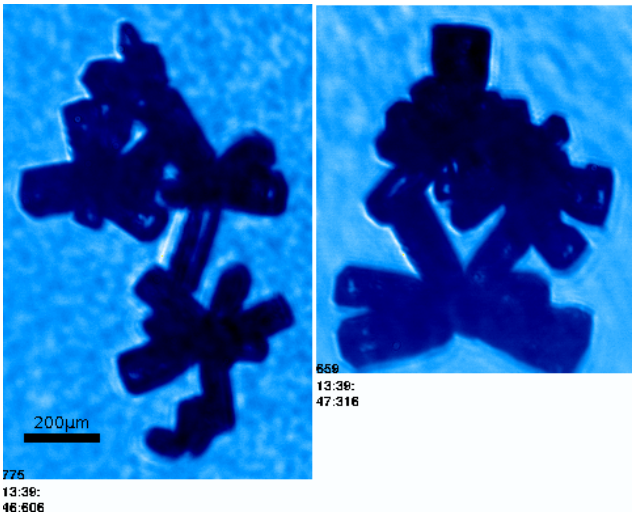

Figure 6. CPI ice crystal images from run 5. Time stamps are indicated below each image.

Atmos. Chem. Phys. Discuss., doi:10.5194/acp-2016-409, 2016
Manuscript under review for journal Atmos. Chem. Phys.
Published: 26 May 2016

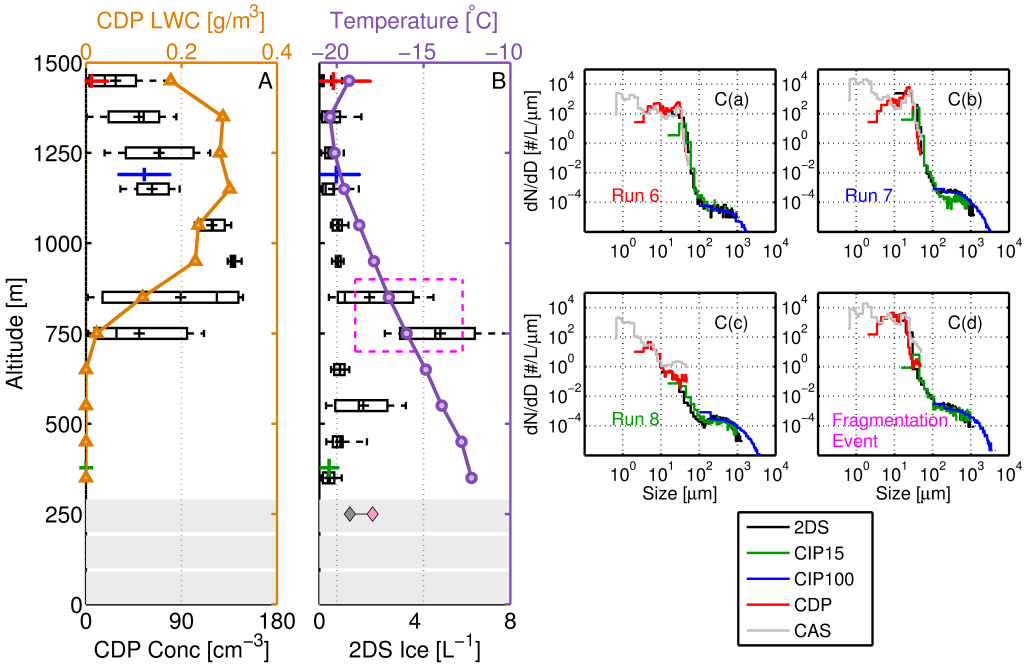

Figure 7. Microphysics summary of averaged observations over the ocean. Data are displayed similarly to Fig. 5. In panels **A** and **B**, data from each SLR are again shown in colour at each corresponding altitude (run 6: red, run 7: blue, run 8: green) as before. Evaluated D10 predictions are indicated (diamonds) in panel **B**. **C(a-d):** Number size distributions (dN/dD) from each SLR over the ocean (runs 6-8). Legend refers to panel **C** only. High ice number concentrations at cloud base are labelled as a fragmentation event (see Sects. 4.1.2 and 5.3).

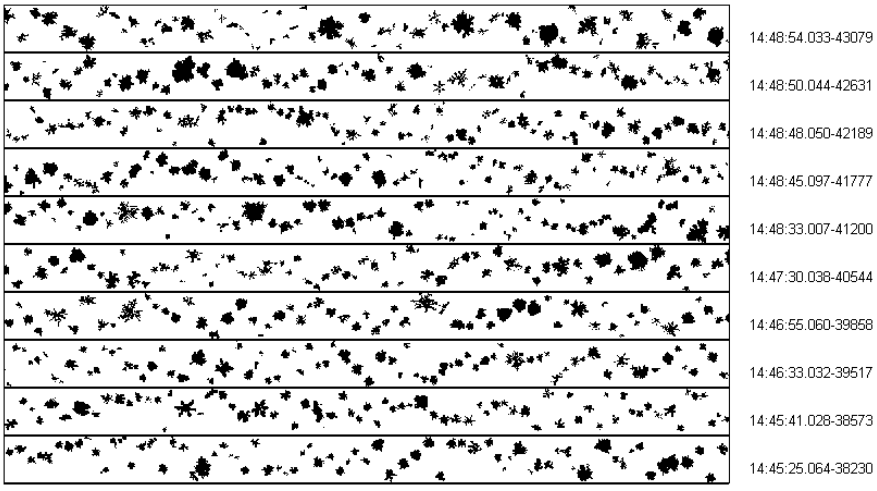

Figure 8. Example CIP100 data from run 8. Vertical width of image strip represents a size range of 6.4 mm.

Atmos. Chem. Phys. Discuss., doi:10.5194/acp-2016-409, 2016
Manuscript under review for journal Atmos. Chem. Phys.
Published: 26 May 2016

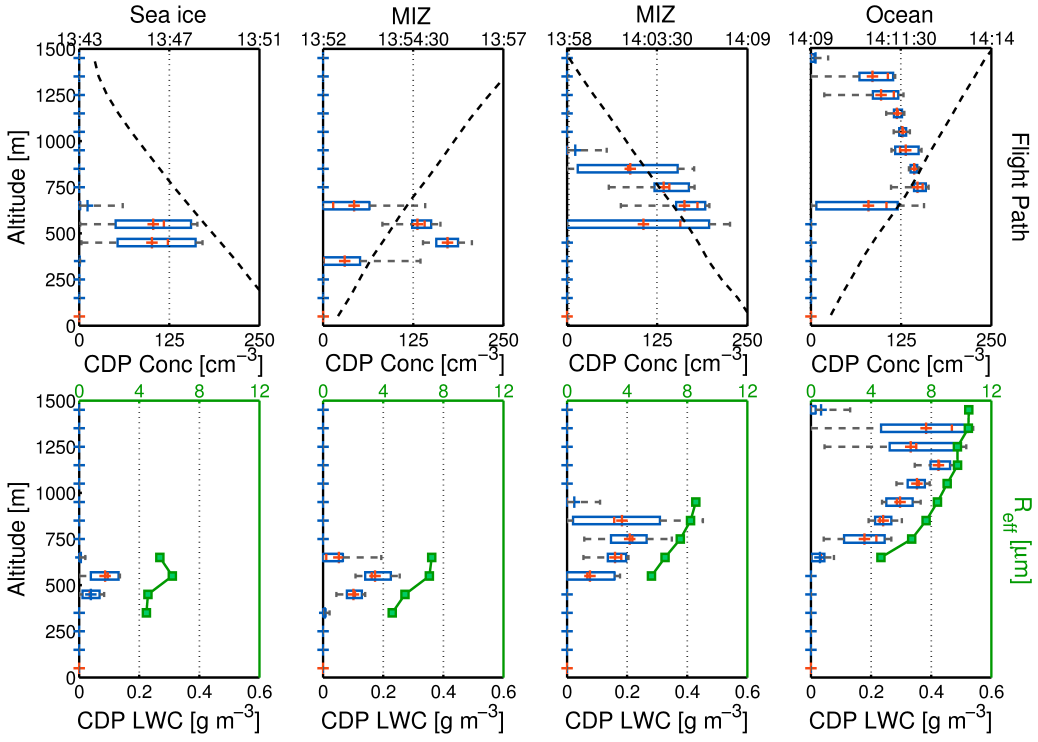

Figure 9. CDP data from the sawtooth profiles. Cloud droplet number concentration (cm^{-3}, **top row**) and derived LWC (g m^{-3}, **bottom row**) are shown. Box edges again indicate the 25 % and 75 % thresholds of the data, mean values are shown as a red cross and outliers extend to the 10 % and 90 % thresholds. The altitude of the aircraft is indicated (black, dashed) in the top row and mean droplet effective radius – in µm, derived from CDP measurements – is shown (green) in the bottom row. Columns indicate the different profiles, transitioning from sea ice to ocean from left to right.

Atmos. Chem. Phys. Discuss., doi:10.5194/acp-2016-409, 2016
Manuscript under review for journal Atmos. Chem. Phys.
Published: 26 May 2016

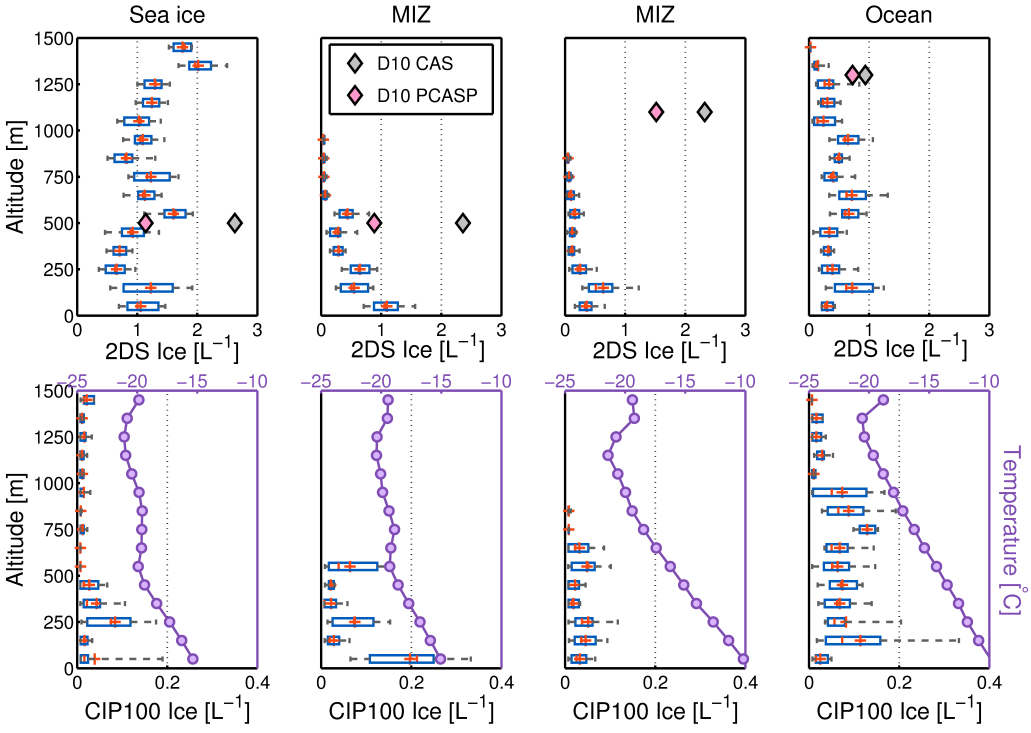

Figure 10. Ice number concentrations (L^{-1}) from the 2DS and CIP100 from the sawtooth profiles over the transition region. Data are displayed similarly to Fig.9. Evaluations of the DeMott et al. (2010) parameterisation using PCASP and CAS-DPOL data >0.5 µm are indicated in the top row, where aerosol data from ±200 m of cloud top are considered in calculating the average. Temperature is overlaid (purple) in the bottom row.

Atmos. Chem. Phys. Discuss., doi:10.5194/acp-2016-409, 2016
Manuscript under review for journal Atmos. Chem. Phys.
Published: 26 May 2016

Atmospheric Chemistry and Physics Discussions

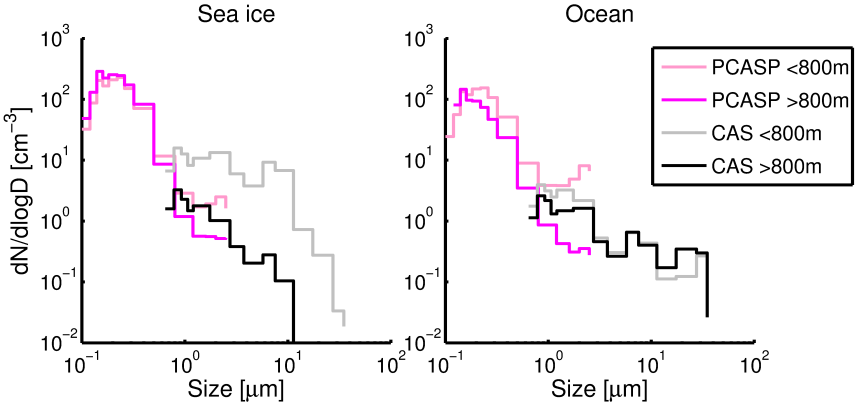

Figure 11. PCASP and CAS-DPOL particle size distributions over sea ice and ocean. Data are split into lower and higher than 800 m to reflect altitude influences. Only out of cloud (CDP LWC$\leq$0.01 g/m^3) data are included.

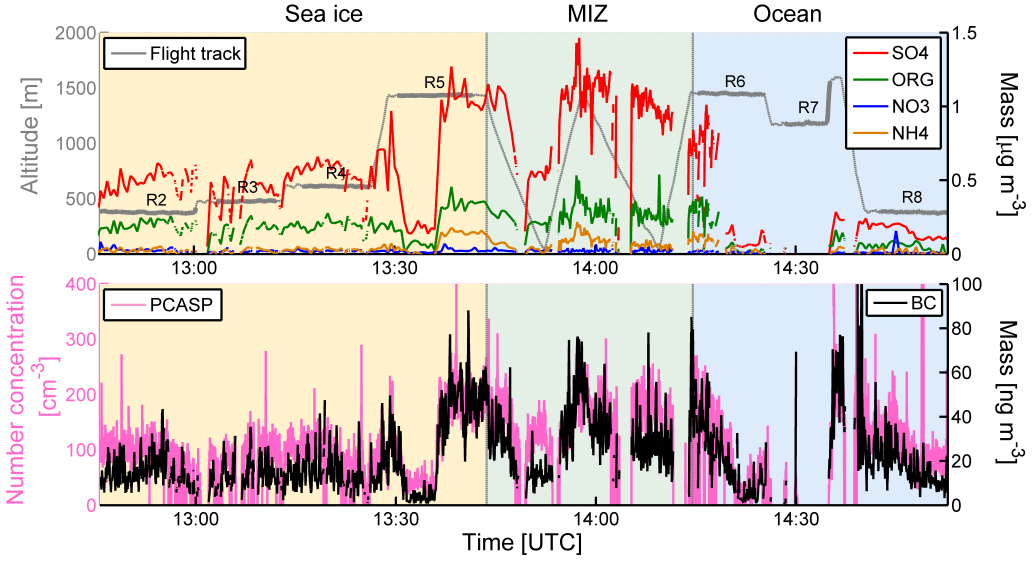

Figure 12. AMS and SP2 mass loading and PCASP number concentration time series. **Top row:** Flight track is shown in grey (with SLRs indicated in bold) with AMS species indicated by the legend in the top right. **Bottom row:** Aerosol number concentration and black carbon mass loading from the PCASP (pink) and SP2 (black) respectively. Only out of cloud (CDP LWC$\leq$0.01 g m^{-3}) data are included.

Atmos. Chem. Phys. Discuss., doi:10.5194/acp-2016-409, 2016
Manuscript under review for journal Atmos. Chem. Phys.
Published: 26 May 2016

Atmospheric Chemistry and Physics Discussions

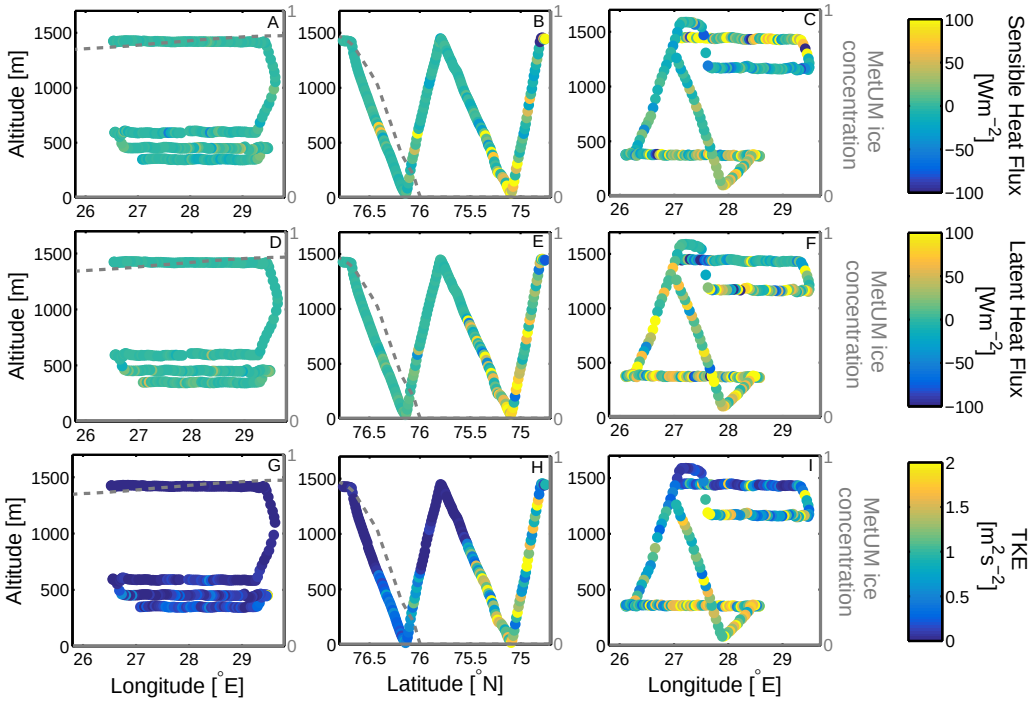

Figure 13. Sensible (**top row**) and latent (**middle row**) heat fluxes and turbulent kinetic energy (TKE, **bottom row**) calculated at 10 s intervals along the flight path. The path of the aircraft with respect to latitude (**middle column**) or longitude (**left-** and **right-hand columns**) is shown, with the measurements indicated in colour. The left column displays data from over the sea ice, whilst the middle and right columns show MIZ and ocean data respectively. Approximate MetUM sea ice fraction is shown (grey, dashed) over the sea ice and MIZ (**left** and **middle columns**), and is absent over the ocean (**right column**).

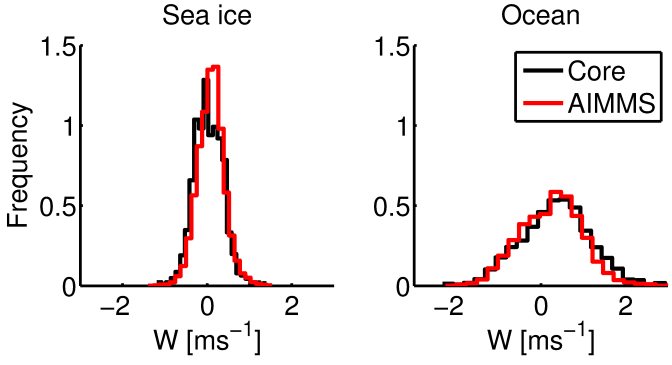

Figure 14. Probability density function (PDF) of updraught velocity from the core turbulence (black) and AIMMS (red) probes. Data from runs 2, 3 and 4 are used for the sea ice; and from runs 6 and 7 for the ocean. Data from each SLR are normalised such that the mean value is zero.